Geochemical Evidence for Initiation of the Modern Mekong Delta in the southwestern South China Sea after 8 Ma

Chang Liu[1], Peter D. Clift[1*], Richard W. Murray[2], Jerzy Blusztajn[3], Thomas Ireland[2], Shiming Wan[4], Weiwei Ding[5]

1 - Department of Geology and Geophysics, Louisiana State University, Baton Rouge 70803, USA

2 - Department of Earth and Environment, Boston University, Boston, MA 02215, USA

3 - Department of Geology and Geophysics, Woods Hole Oceanographic Institution, Woods Hole, MA 02540, USA

4 - Key Laboratory of Marine Geology and Environment, Institute of Oceanology, Chinese Academy of Sciences, Qingdao 266071, China

5 - The Second Institute of Oceanography, State Oceanic Administration, Hangzhou 310012, China

Abstract

Sedimentary records in the southwestern South China Sea reflect the evolving erosion and drainage systems that have operated in Southeast Asia during the Neogene. Analyses of the chemistry and clay mineral composition of sediments from International Ocean Discovery Program (IODP) Site U1433 allow us to examine these processes over the last 17 Ma. Sediment

* Corresponding author: pclift@lsu.edu

older than 8 Ma was deposited relatively slowly. Sr and Nd isotopes indicate a variable provenance with sequences of less and more altered material accompanied by strong changes in the proportion of smectite. Sediment flux was probably from Indochina, as well as from a more primitive volcanic source, most likely the Palawan ophiolite and/or Luzon. Sediments younger than 8 Ma show a more stable Sr and Nd isotope character, indicating sources close to those seen in the modern Mekong River, although with some influx from smaller rivers draining the Indochina margin especially from 4–8 Ma. Our data are consistent with seismic estimates for an onset to the Mekong in its present location after 8 Ma, following an avulsion from the Gulf of Thailand.

Keywords: Geochemistry; clay minerals; isotopes; provenance

1. Introduction

Erosion and chemical weathering are primary processes that drive recycling of the continental crust and the generation of the sedimentary record (Clift et al., 2009; McLennan, 1993). Nonetheless, debate continues concerning what factors are most influential in controlling erosion and weathering and how quickly these respond to tectonic and climatic forcing (Burbank et al., 2003; Lavé and Avouac, 2001; Liu et al., 2005; Riebe et al., 2001; Wobus et al., 2010). Southeast Asia is a good location to investigate such issues because of the strong forcing of the East Asian monsoon, which dominates the climate of the area. Much of the sediment that has been eroded from the Asian continent, some from the edge of the Tibetan Plateau, is delivered into the South China Sea by a number of small and well-known larger river systems, including the Pearl, Red,

and Mekong (Fig. 1). This has resulted in the accumulation of large volumes of sediment around the continental margins of the South China Sea (Métivier et al., 1999).

Sediment provenance and delivery rates are complicated by the fact that there has been substantial drainage reorganization in Southeast Asia, probably driven by the progressive uplift of Asian topography, which has resulted in head water capture and the diversion of river systems into different parts of the continental margin during the Cenozoic (Clark et al., 2004; Clift et al., 2006a; Zheng et al., 2013). Unless the changing source of sediment can be deciphered, using reconstructions of chemical weathering to infer continental environmental change is potentially unreliable because varying source compositions may overprint the effects of the climatically driven weathering.

In this study we examined sediment from a new scientific drilling site in the central southwestern part of the deep-water basin (Fig. 1) and attempted to reconstruct both the sources of the sediment since ~17 Ma, and to assess the varying degrees of chemical weathering, in order to understand how tectonism and changing climate may have impacted the sediment of the deep-water basin, as well as environmental conditions in the source regions.

1.1 Geological Setting

Our study exploits sediment cored at International Ocean Discovery Program (IODP) Site U1433 (Li et al., 2015), located in the southwestern part of the South China Sea basin. The South China Sea itself initially began to extend in the latest Cretaceous (Cullen et al., 2010), but underwent the main phase of continental rifting in the Eocene (Ru and Pigott, 1986; Su et al., 1989), culminating in the onset of seafloor spreading around 30 Ma (Briais et al., 1993). Study of paleomagnetic data has resulted in a debate about when active seafloor spreading ceased

(Barckhausen et al., 2014), but drilling during IODP Expedition 349 now demonstrates that this finished at ~15–16 Ma (Li et al., 2014). Site U1433 overlies an oceanic basaltic basement dated at ~17 Ma (Li et al., 2015), and seafloor spreading in the basin finished shortly after the eruption of this basement.

The causes of the extension itself have been widely debated and have involved relative shear between Indochina and mainland China as a result of the left lateral extrusion of Indochina along the Red River Fault Zone (Replumaz and Tapponnier, 2003; Tapponnier et al., 1982). Alternatively, others have invoked subduction-related forces towards the south, causing the Dangerous Grounds continental block to rift from mainland Asia and subsequently collide with Borneo closing an earlier paleo-South China Sea basin ~16 Ma (Clift et al., 2008; Hutchison, 2004; Morley, 2002; Taylor and Hayes, 1983). Since the Middle Miocene the tectonics of the basin have been relatively inactive, with the exception of active subduction along the eastern side where the South China Sea lithosphere is subducting beneath the Philippine arc (Hayes and Lewis, 1984). There have also been intraplate tectonic activities, most notably the uplift of the Vietnamese Central Highlands and the extrusion of a thick basaltic sequence, mostly after ~8 Ma (Carter et al., 2000; Cung et al., 1998), although with lesser volumes of lava also being emplaced in the Early and Middle Miocene (Hoang and Flower, 1998; Wang et al., 2001). Compression along the southern side of the basin, along the northern coast and continental margin of Borneo, appears to be only slightly active in the present day (Hinz et al., 1989; Simons et al., 2007).

The relatively central location of Site U1433 within the oceanic basin means that several possible sources may have provided sediment to this location in the geologic past.

Our working hypothesis was that the largest river in Southeast Asia, namely the Mekong, might be the primary source of sediment to the site, at least in the recent past, since this had been

implicated as the primary source to Ocean Drilling Program (ODP) Site 1143, which is located only ~450 km to the southeast (Wan et al., 2006)(Fig. 1). This largely reflects the substantial discharge from the Mekong, ~166 mT/yr (Milliman and Syvitski, 1992) and also the fact that other potential sources, such as Luzon or Borneo, are isolated from the site by significant bathymetric features such as the Manila Trench and the Sabah Trough (Fig. 1). However, estimated average annual discharge of ~459 and 498 mT/yr respectively from North Borneo and from Sumatra (Milliman et al., 1999) raises the possibility that these may have been important sources in the past. However, because these values are modeled, not measured, they may be over-estimates, as implied by more recent estimates of ~30 mT/yr for the Rajang River, the largest in northern Borneo (Milliman and Farnsworth, 2011). Furthermore, seafloor samples north of Reed Bank (~190 km to the east of the site), have relatively primitive ε_{Nd} values (-3.1)(Wei et al., 2012) and >40% smectite contents suggestive of dominant supply from Luzon (Liu et al., 2016b) in recent times.

We were interested to test the concept that the Mekong River had a relatively recent initiation. A secondary objective was to test the erosional and weathering response within the Mekong basin of changes in monsoon intensity since the beginning of the Middle Miocene. Seismic data collected close to the Vietnamese coast, as well as on the continental margin, suggests that the modern submarine delta might be relatively young, initiating in the Pliocene (Li et al., 2013; Murray and Dorobek, 2004) and at odds with evidence from the other major rivers in eastern Asia that suggest large-scale drainage capture in the Early Miocene (Clift et al., 2006a; Zheng et al., 2013).

Age control at the drill site was provided through a combination of biostratigraphic and magnetostratigraphic data (Li et al., 2015) that allowed us to select samples evenly spaced in

time and spanning the entire basin history. The sediments overlying the basement are almost 800 m thick and are dominated by massive and bioturbated muds and mudstones, largely clays, but with a significant proportion of fine silt which are interpreted as turbidites. These sediments are interbedded with graded calcareous turbidites, at least until the upper 250 m of the section (Pleistocene) where mudstones dominated entirely (Fig. 2)(Li et al., 2015). At the microscopic level, the clay-rich sediment are seen to contain minor but significant quantities of opaque material and fine silt–sized quartz, as well as some lithic grains, chert and feldspar. Fragments of angular, mafic, volcanic glass are also observed at very low concentrations. The bulk of the intercalated sediment is redeposited carbonate, likely derived from the reef areas of the Dangerous Grounds and the Reed Bank to the south. Over some intervals carbonate dominates, but we only focus on the clastic fraction. Over the basal 49 m of the section the sediment is a reddish brown claystone with very minor silt and no calcareous microfossils in a deposit similar to those seen in the central Pacific basin.

1.2 Sediment Provenance in the South China Sea

In order to reconstruct erosion patterns and changes in sediment supply we first need to identify specific characteristics that allow us to assign clastic sedimentary particles to particular bedrock sources, something which is possible in Southeast Asia as a result of the diversity of possible source terrains that surround the South China Sea (Clift, 2015). The ability to distinguish and estimate the amount of sediment derived from a given source is based on the concept that the bedrock sources providing the sediment differ from one another, either in terms

of their chemistry, geochronology or tectonic evolution. These differences are then transferred from the bedrock to the sediment in the rivers and thus to the offshore.

The tectonic blocks of SE Asia were largely brought into juxtaposition during the Triassic Indosinian Orogeny (Carter et al., 2001; Lepvrier et al., 2004). Because of their contrasting geological histories, the various tectonic blocks produce sediment of different composition, which can then be detected in the sediments deposited at Site U1433. The geological evolution of each of these blocks is relatively complicated, but in general southern China (Cathaysia), represents a tectonic block that collided with the Yangtze Craton ~800 Ma and later was the host to a Mesozoic volcanic arc complex (Fletcher et al., 2004; Jahn et al., 1990). Other tectonic blocks were rifted from Gondwana and accreted to Asia largely during the Triassic (Metcalfe, 1996). These have been later overprinted by younger events, although the old age of the basement has remained undisturbed. Consideration of radiogenic isotopes, especially Sr and Nd, in the rivers of Southeast Asia suggests that there are resolvable differences between the large blocks draining the Pearl, Red and Mekong Rivers (Liu et al., 2007).

An alternative approach to provenance may involve consideration of the bulk sediment geochemistry and clay mineral assemblages, which are known to be different in different parts the South China Sea. Chemical weathering intensity is generally high in the tectonically inactive Pearl River basin and is less pronounced in the Mekong and lower still in the Red River (Liu et al., 2007). Chemical weathering is also high in the Malay Peninsula and in Sumatra (Liu et al., 2012). In the present day certain source terranes are associated with high concentrations of particular clay minerals. Erosion of the volcanic terrains in Luzon in the Philippines is marked by high concentrations of smectite (Liu et al., 2009b), whereas erosion from Taiwan is marked by sediment rich in illite and chlorite (Liu et al., 2008). Kaolinite is associated with the Pearl River,

as well as rivers draining the Malay Peninsula, Sumatra, and to a lesser extent Western Borneo (Liu et al., 2012). However, care should be taken when using clay minerals alone as provenance proxies because they are also affected by environmental/climate conditions so that a particular river will typically not have a stable clay mineral composition over long periods of geological time (Hu et al., 2013). In addition, clay minerals may be subject to sorting by differential flocculation during transport within a river mouth or the nearshore environments (Edzwald and O'Melia, 1975; Gibbs, 1977).

2. Analytical Methods

One hundred bulk sediment samples were selected in order to provide an even distribution through the entire age of the sequence at IODP Site U1433. Samples were first decarbonated using 0.5% acetic acid. Decarbonation lasted for 3-4 days until no further fizzing was observed with new acid. Samples were washed by deionized water before being ground into powders. Approximately, 0.1 gram of sample was mixed with 0.4 gram of $LiBO_2$ and heated in an oven at 1500˚C. The melted samples were dissolved in 3% ultraclean HNO_3, ultrasonicated, dissolved, and diluted for analysis. The major element composition (Table 1) was determined by Inductively Coupled Plasma Emission Spectrometry (ICP-ES) at Boston University, with precision quantified to be better than 2% of the measured value for all elements. Accuracy was constrained by analysis of certified Standard Reference Materials (BHVO-2), and results were accurate within precision. Table S1 (online supplementary information) provides the results of the repeated analyses of the standard and of the replicate analyses of Samples U1433B-60R-2, 45-47 cm and 63R-1, 39-43 cm.

Thirty two of the 100 decarbonated samples were also analyzed to determine $^{143}Nd/^{144}Nd$ and $^{86}Sr/^{87}Sr$ values (Table 2). Prior to total digestion, all samples were leached again using buffered acetic acid to remove any carbonate-bound Sr. Samples were digested using a standard HF-HNO_3 technique. For Sr and Nd separation samples were dissolved in 3:1 mixture of concentrated HF and HNO_3 on hot plate at 100˚C for at least 24 hr, followed by three dry downs in 6.2 N HCl. Prior to loading onto the ion exchange columns, samples were centrifuged to remove any residual graphite. Solutions were loaded on to Sr-spec resin in order to separate Sr isotopes, following the procedure outlined by Deniel and Pin (2001). One-step column chemistry utilizing Ln resin was used for Nd separation. Nd and Sr isotopic compositions were determined by Finnigan Neptune multi-collector inductively coupled plasma mass spectrometer (MC-ICP-MS) at Woods Hole Oceanographic Institution. Nd and Sr isotope analyses were corrected against La Jolla Nd standard $^{143}Nd/^{144}Nd=0.511847$ and NBS987 standard $^{87}Sr/^{86}Sr=0.710240$. Procedural blanks for analyses were 20–25 pg for Sr (and 50–70 pg for Nd). The standard NBS 987 was run to monitor machine performance and yielded an average $^{87}Sr/^{86}Sr$ of 0.710254 ± 18 (27 ppm 2σ, n=24), which is within error of the multi-dynamic TIMS value of $^{87}Sr/^{86}Sr$ = 0.710248 ± 11 reported by Thirlwall (1991). Nd isotope analyses were corrected against La Jolla Nd standard $^{143}Nd/^{144}Nd=0.511839 \pm 10$ 2σ. We calculate the parameter ε_{Nd} (DePaolo and Wasserburg, 1976) using a $^{143}Nd/^{144}Nd$ value of 0.512638 for the Chondritic Uniform Reservoir (CHUR (Hamilton et al., 1983)). Data is provided in Table 2. Because our samples are generally fine grained and thus homogenous, especially after powdering, we did not anticipate that there would be high errors in external reproducibility. Nonetheless, because very small proportions of monazite/allanite control Nd isotopes (Garçon et al., 2014) samples were dissolved until no residue was visible. To verify the magnitude of the external reproducibility we measured two of

200 the samples three times each for Nd isotopes and twice for Sr in order to assess the uncertainty
201 (Table 2). We found that ε_{Nd} values only varied by 0.2 points between the repeats while $^{87}Sr/^{86}Sr$
202 values differed by ~0.00004.

203 Clay mineralogy was determined by using X-Ray Powder Diffraction (XRD) at
204 Louisiana State University using a Panalytical Empyrean X-Ray Diffractometer. The same 100
205 samples were soaked in water until there was no flocculation, with Na_3PO_4 added to de-
206 flocculate when necessary. Four XRD patterns were generated from each oriented sample smear.
207 The first was collected from the sample in air-dried condition. The slide was then placed in a
208 desiccator with ethylene glycol for a minimum of eight hours at 25˚C, and the second XRD
209 pattern was generated from a glycolated sample. The third and fourth XRD data sets were
210 collected after the sample was subjected to heat treatments of 300˚C for one hour, and then
211 550˚C for one hour, respectively. XRD analysis began immediately after glycolation, and
212 immediately after the first heat treatment. In this study we use the semi-quantitative method of
213 Biscaye (1965) to estimate the clay assemblage, which is based on peak-intensity factors
214 determined from calculated XRD patterns as measured by MACDIFF software. For clay
215 minerals present in amounts >10 wt % uncertainty is estimated as better than ±5 wt % at the 95%
216 confidence level. Uncertainty of peak area measurement based on repeated measurements is
217 typically <5%. We further calculate the illite chemistry index (the ratio of 5 Å and 10 Å peak
218 areas), and illite crystallinity (the full width at half maximum height of the illite 10 Å peak)
219 determined on the glycolated curve. Illite chemistry indexes below 0.15 represent Fe-Mg-rich
220 illites (biotite, mica) characterized by physical erosion, whereas indexes above 0.4 are primarily
221 found in Al-rich illites (muscovite) formed by strong hydrolysis (Petschick et al., 1996). In
222 addition to calculating the relative concentrations of clay minerals in the samples, we also

223 determine various ratios based on measurements of peak areas in the XRD patterns. These ratios
224 are used to reconstruct changes in relative abundance and are directly proportional to ratios
225 calculated from the exact values for individual mineral concentrations. Data are presented as
226 relative concentrations of the total clay assemblage in Table 3.

227

228 **3. Results**

229 Selected results of the geochemical analysis are shown with the sedimentary log in Figure 2.
230 We use the widely applied chemical index of alteration (CIA; Nesbitt and Young (1982)) to
231 quantify weathering intensity. The CIA was developed for soils but is often applied to marine
232 sediments in order to assess the degree of chemical breakdown compared to fresh bedrock. This
233 proxy is calculated using the following formula, based on the notion that Ca, Na and K are
234 depleted in most sediments as a result of chemical weathering, although recognizing that Na may
235 be more immobile in clays (Nesbitt et al., 1980):

$$CIA = \frac{Al_2O_3}{Al_2O_3 + CaO^* + Na_2O + K_2O}$$

236 where CaO* is the calcium content from the silicate fraction of the sediment corrected for
237 phosphate contents (Singh et al., 2005). Because the sediments were decarbonated there is little
238 difference between CIA values derived using the phosphate correction or not and the trends are
239 similar. We slightly prefer the Singh et al. (2005) method as a way to insure against the
240 possibility of residual carbonate left after acid treatment. High CIA values are visible around 600
241 meters below seafloor (mbsf) and again around 350 mbsf (Fig. 2), above which level the values
242 tend to decrease towards the seafloor. The seafloor itself shows a relatively unweathered

243 composition. Variations in the Chemical Index of Alteration of the sediment through time are
244 shown in Figure 3. CIA values before 8 Ma show some cyclicity with higher and lower values on
245 timescales of around 2 m.y. From 8 Ma to 6 Ma CIA is essentially constant, followed by a 2 m.y,
246 long increase in CIA to ~4 Ma, in turn followed by a progressive decrease to the present day. We
247 also plot Ni/Zr as a proxy for the involvement of Ni-rich mafic and ultramafic igneous rocks
248 compared with zircon-bearing Zr-rich granitic continental rocks. This ratio is high at 17 Ma and
249 then falls mostly progressively until ~10 Ma. It remains largely constant through the past 8 Ma
250 (Fig. 3).

251 Both Sr and Nd isotopes show similar and consistent variability with depth. There is a
252 zone below 700 mbsf with low values in $^{87}Sr/^{86}Sr$ (0.71–0.72), as well as less negative ε_{Nd} values
253 (-5 to -8). Above 700 mbsf there is a change in both isotope systems with a long-scale decrease
254 of $^{87}Sr/^{86}Sr$ values from >0.73 at 700 mbsf to ~0.723 at the seafloor. ε_{Nd} seems to be slightly
255 more consistent at a level of ~ -11 shallower than 700 mbsf. There is a brief departure to lower
256 $^{87}Sr/^{86}Sr$ values and more positive ε_{Nd} visible between 400 and 500 mbsf above which level the
257 isotope ratios return to that seen below 500 mbsf.

258 Clay minerals show consistent changes through the sequence (Fig. 2). Smectite is
259 particularly abundant below ~680 mbsf, above which level it falls in a consistent fashion towards
260 around 160 mbsf, being more constant at shallower depths. Chlorite and kaolinite are relatively
261 scarce in the sequence, especially towards the bottom where they form a small fraction of the
262 total clay assemblage. They rise in abundance above 680 mbsf but remain less than 20% of the
263 total assemblage. Illite is the second most abundant clay mineral in the sediments and shows a
264 reverse trend to that seen in the smectite, being low at the base of the sequence and rising
265 steadily up-section, reaching a level of around 40% close to the seafloor. Because the total clay

assemblage is normalized to 100% the increase in illite up-section may simply reflect less smectite. Many of the clay mineral abundances appear to be less variable in the upper 250 m of the section, although sampling density was less because of the higher sedimentation rate.

4. Discussion

4.1 Chemical Weathering Proxies

While changes in CIA measured alteration intensity and may be linked to climate change causing changes in weathering rates grain size variations may also control this proxy, reflecting the fact that some of the sediments are silty turbidites, coarser than the dominant muds. We use Si/Al as a proxy for the grainsize of the sediment because quartz sand has higher Si/Al values than silt which is turn has higher values than clays (Lupker et al., 2011). Temporal variations in Si/Al, and in Si alone, are similar to those in CIA (Fig. 4), suggesting that there is close link between quartz sand content and degree of alteration. This is not a direct consequence of the presence of quartz but rather the loss of unstable minerals. For example, the silt fraction may contain abundant micas that have lower CIA values than clays (Andrews et al., 2013). Quartz-rich sediment tends to be less altered than clay-rich material, which is consistent with earlier studies (Hoang et al., 2009) and the idea that clay is itself an alteration product. Consequently we do not consider CIA to be a good tracer of environmental conditions in the source regions in this case.

Clay mineral assemblages may also be used to interpret paleo-weathering conditions, because these are unaffected by other coarser mineral species. Clays have been used to examine changes in weathering assuming that clay mineral formation is a direct response to

288 environmental conditions (Thiry, 2000). Soil forms rapidly and to greater depths in tropical and
289 subtropical environments, where chemical weathering is intensified by the process of leaching
290 (Birkeland, 1984). As a result, kaolin-group minerals are frequently abundant in well-developed
291 (meters thick) soils from regions of tropical climate with high rainfall, whereas warm regions
292 with more seasonality and thus with less leaching, are more prone to producing smectite-rich soil
293 (Hillier, 1995).

294 Clay mineral records from the South China Sea show a good correspondence between
295 clay assemblages and the intensity of the East Asian monsoon over periods $>10^6$ yr (Wan et al.,
296 2007). Recently, it has also been suggested that changes in mineralogy linked to millennial-scale
297 variations are recorded in sediments from other Asian continental margins (Boulay et al., 2007;
298 Colin et al., 2010; Liu et al., 2010; Liu et al., 2005), implying that the clay minerals in a
299 weathering system can respond and leave a record even on time scales much shorter than those
300 considered here.

301 Temporal evolution in smectite/(illite + chlorite) and kaolinite/(illite + chlorite) is shown
302 in Figure 3. Prior to 8 Ma there is significant variation in the record, with particularly high
303 relative abundances of smectite seen around 9, 12 and 15.5 Ma. Several of the changes in the
304 relative abundance of smectite correlate with times of change in the Nd- and Sr isotopes,
305 suggestive of a provenance control, as discussed below.

306

307 *4.2 Provenance*

308 *4.2.1 Major and Trace Elements Constraints*

The progressive evolution in Ni/Zr suggests stronger erosion from Ni-bearing rocks prior to 12 Ma and lesser involvement from typical granitic zircon rich sources. Ni is most common ultramafic and mafic igneous rocks. Mielke (1979) reported values for Ni in igneous rocks as: ultramafic 2000 mg kg-1, basaltic 130 mg kg-1 and granitic 4.5-15 mg kg-1. This is supportive of some mafic igneous, possibly ophiolitic source in the early stages of the basin sedimentation. We explore this further with simple trace element discrimination diagrams. Figure 5A, from Hiscott (1984) shows that a typical ophiolitic source including peridotites and other deep crustal ultramafic would be expected to have high Cr/V and low Y/Ni values. The sediments from Site U1433 scatter between the Post-Archean Australian Shale (PAAS, a proxy for fine grained sediment derived by erosion of the upper crust) and Upper Continental Crust averages of Taylor and McLennan(1985). The samples show little indication of strong ophiolitic involvement and are in many respect typical of erosion from continental sources.

Use of the TiO_2 versus Zr plot of Nagarajan et al. (2014), designed for analysis of sediments in Borneo further reinforces this provenance interpretation (Fig. 5B). With a small number of extreme exceptions the sediments plot on the boundary between the felsic and intermediate rock fields, consistent with a general continental source and ruling out a dominant flux from mafic igneous sources around the South China Sea, such as Luzon, Palawan or the Vietnamese Central Highlands.

4.2.2 Isotope Character and Provenance

We further address provenance through Nd- and Sr isotopic data (Fig. 3). Close similarities are noted in the general shape of Sr and Nd curves through time, with both showing a

sharp change close to 8 Ma, with lower ε_{Nd} values and higher $^{87}Sr/^{86}Sr$ values dominating after that time. The change is especially striking in terms of $^{87}Sr/^{86}Sr$. Before 8 Ma there is significant variability, with phases of greater stability in isotope character separated by times of rapid change.

Recent work shows that the Nd content of sediment is largely controlled by the presence of monazite and allanite, which are not separated by mineral sorting and the Nd-isotopic signal is thus relatively insensitive to hydrodynamic sorting during transport (Garçon et al., 2013; Garçon et al., 2014). Moreover, because the Nd- and Sr-isotopic signals are similar this suggests that the Sr signal is not significantly affected by chemical weathering or by mineral sorting during transport in this particular case, as marked by the strong inverse correlation shown in Figure 6 (correlation coefficient R2=0.77).

We can better constrain provenance by comparing sedimentary values with those known from potential source areas. The sediment at Site U1433 is close to the modern Mekong River in ε_{Nd} values after 8 Ma (Fig. 6), although the $^{87}Sr/^{86}Sr$ values are higher than the modern river sediments during this time period. This may imply input from the Mekong River system to the deep South China Sea. ε_{Nd} values change from being more positive than the modern Mekong in sediments older than 9 Ma to being more negative, or within the range of modern river sediments, in those younger than 8 Ma. Before 9 Ma source variation was significant and seems to correlate with CIA and some clay mineral ratios (Fig. 3). Relatively positive ε_{Nd} values before 9 Ma are indicative of sediment input from very different sources than those that have dominated the area since 8 Ma. The positive ε_{Nd} values require input from relatively juvenile sources rather than older continental crust, which is more important in the younger part of the record.

A number of possible sources could account for the range of sediment isotope compositions in the deep SW basin, although some are better characterized than others. In Borneo there is no isotopic information concerning possible bedrock sources from the onshore itself, so we are forced to infer possible source compositions from the modern shelf sediment, although this is poorly defined on the basis of a small number of samples around its coast (Wei et al., 2012). Borneo is unlikely to be a major supplier of sediment to Site U1433 because of the bathymetric barriers that separate it from the deep South China Sea, favoring most sediment being preserved closer to source. Seasonal currents also tend to move suspended sediment to the NE and SE and not towards Site U1433. Similarly, the Red River is not a practical source of sediment to Site U1433 because it lies too far to the north and sediment from this river is captured in the Song Hong-Yinggehai Basin, as well as the Xisha Trough in the northern South China Sea. Modern Taiwanese river sediments span a range of Sr and Nd isotope values that are similar to the Site U1433 sediments but generally plot with lower $^{87}Sr/^{86}Sr$ values. The great distance between the site and Taiwan, as well as the opposing summer surface currents tend to argue against this is being a major supplier to the area.

Small coastal rivers draining Indochina also have high $^{87}Sr/^{86}Sr$ values and relatively negative ε_{Nd} values. A study of the Song Gianh, which drains the coastal Annamite Range at ~18˚N (Jonell et al., 2016), shows the potential of such rivers to act as suppliers of clastic sediment to the drill site. The Song Gianh itself is located too far north to have been a significant source, but similar rivers located further south, and also eroding Indochina basement, might provide isotopically similar material to the drill site where they could mix with sediment from other sources. Such transport would be favored by the narrow continental shelf located offshore

375 southern Vietnam. Possible influence of such Annamite sources is strongest in the younger
376 samples (<8 Ma) with $^{87}Sr/^{86}Sr$ values higher than those known in the modern Mekong.

377 The modern Mekong River is a likely dominant source of sediment to the site in more
378 recent geological times given its proximity to the shelf edge of the SW basin and the clear
379 sediment transport pathway. The known isotopic range of sediments in the modern Mekong is
380 relatively restricted, but has lower $^{87}Sr/^{86}Sr$ values and slightly higher ε_{Nd} values compared to
381 many of the analyses that postdate 8 Ma. This means that the sediment at Site U1433 cannot be
382 exclusively derived from the Mekong. The past composition of the Mekong River is, however,
383 presently unconstrained and this requires us to use the modern river as an approximate estimate
384 for the long-term input. The Mekong itself likely changed composition in the past, possibly
385 because of changing drainage basin geometry and chemical weathering/environmental conditions.
386 The post-8 Ma samples fall between the range of the Mekong River and Annamite Range rivers,
387 indicating that a mixture between these sources could account for the measured ratios. Input
388 from other sources is possible but likely to be small after 8 Ma.

389 The influence of the Pearl River can also be considered although sediment from the river
390 now largely moves to the west of its delta towards Hainan (Liu et al., 2009a) and the river is both
391 far from the drill site and separated from it by the relict oceanic ridge. The Pearl River is
392 presently highly anthropogenically impacted so that its modern samples are elevated in $^{87}Sr/^{86}Sr$
393 compared to the natural state. We use the range of Holocene analyses from the Pearl River
394 mouth from Hu et al.(2013) rather than the modern samples of Liu et al.(2007) because that
395 study eliminated the anthropogenic effect and more importantly capture the composition of the
396 river entering the South China Sea rather than identifying end member tributaries in the
397 headwaters whose extreme compositions were likely never delivered to the delta in an undiluted

form. The Pearl River delta plots around the Mekong samples, making it impossible to resolve the two based on this method alone. Although Liu et al. (2007) suggested that the modern rivers could be distinguished on the basis of Sr and Nd isotopes consideration of the entire Holocene compositional range of the Pearl River now demonstrates that this is not possible (Hu et al., 2013).

Samples older than 8 Ma are more complex to interpret and are more variable. These show lower $^{87}Sr/^{86}Sr$ values and less negative ε_{Nd} values than the Mekong, and could represent mixture from a number of sources, including the Annamite Range (Indochina), Borneo, and possibly a paleo-Mekong, as well as more primitive volcanic sources. The highest ε_{Nd} value seen in the 12–18 Ma sediments cannot be explained by mixing of Indochina-derived sediment and Borneo-derived sediment (Fig. 6). This implies some sediment delivery from an even more primitive source. In any case, significant erosion from Borneo prior to 12 Ma seems unlikely, because although collision between Dangerous Grounds and Borneo ~16 Ma was driving uplift, this started first in the south of that island, with the North only uplifting in the Late Miocene (Honza et al., 2000; Hutchison, 2005).

The basement of the Dangerous Grounds themselves has been locally dredged and found to be igneous (diorite and olivine gabbro) (Hutchison and Vijayan, 2010). The Dangerous Grounds are now submerged and have likely been submarine through the time of sedimentation at Site U1433, coinciding with the collision between Borneo and Dangerous Grounds (Clift et al., 2008; Hutchison, 2005). Consequently it is unlikely that this block could have been a significant source of sediment to Site U1433.

Erosion from Hainan .could explain the low $^{87}Sr/^{86}Sr$ values before 8 Ma but this island appears to have experienced most of its uplift during the Plio-Pleistocene and was probably not being heavily eroded before 8 Ma (Shi et al., 2011). Possible volcanic sources exist in the seamounts of the South China Sea itself (likely with low $^{87}Sr/^{86}Sr$ and high ε_{Nd} values) and the drill site is located close to some prominent features that were emplaced along the old seafloor spreading axis. Other possible primitive sources could include the volcanic rocks of the Central Highlands of Vietnam. However, these largely erupted after 8 Ma, when this area was rapidly uplifted and dissected (Carter et al., 2000), and therefore these sources cannot explain the isotope excursions seen in the pre-8 Ma record.

Thus a number of possible sources could contribute to the pre-8 Ma sediments. The Luzon Arc is a possible contributor but large volumes of flux are unlikely because it was distant (~950 km today, cf., 730 km from the Mekong Mouth) and located to the SE of the present location at that time as a result of the ongoing subduction under the Philippine (Hall, 2002). Summer surface currents in the modern South China Sea are dominantly flowing to the NE (Chu and Li, 2000), which also argues against significant fine grained sediment transport from Luzon. Transport by bottom or turbidity currents from Luzon is less likely because of the existence of major bathymetric barriers such as the Manila Trench. Nonetheless, mixing with an end member within the Luzon isotopic range could explain some of the isotopic variability seen in the samples older than 8 Ma (Fig. 6).

Sediment from Sumatra could have been a contributor to the total budget, especially given the high modern discharge from this region, but again this was located far to the SW of the drill site (Fig. 7). Although the Sunda Shelf was exposed and able to transport material from Sumatra and the Malay Peninsula via streams such as the Molengraaff River (Molengraaff and

Weber, 1919) during recent glacial low stands it is unlikely that this would have been possible prior to 8 Ma when sea level was significantly higher (Haq et al., 1987).

We favor modest input from Palawan as a possible source of sediment with low $^{87}Sr/^{86}Sr$ and positive ε_{Nd} values. Although there is limited isotopic data from this island (one sample from Fang et al. (1992)), Palawan island exposes ophiolite rocks with suitable isotopic values that could account for some of the range seen at Site U1433. This ophiolite was emplaced on to continental crust in the Oligocene to Early Miocene (Aurelio et al., 2013; Savva et al., 2014) and would have been available for erosion at the time of sedimentation. Although southern Palawan is partly separated from the deep basin by the Sabah Trough, the northern parts of the island would have had a direct transport pathway (~500 km long) downslope towards Site U1433 after the collision between Dangerous Grounds and Borneo-Palawan. Flux from Palawan cannot have been too strong from the ultramafic base of the ophiolite, when we consider the low Cr/V values of the sediment (Fig. 5A).

We try to estimate the possible role of primitive volcanic rocks by constructing mixing lines between an Indochina end member and both Palawan and Luzon Arc end members (Fig. 6), since together these can account for the range of variability seen in the sediments. Mixing only between Indochina and Palawan can explain some of the variability, but many of the sediments plot above the mixing line, indicating that at least one more source is needed to explain all the variability, possibly Luzon. Sedimentation rates prior to 8 Ma were generally low and it is possible that the positive ε_{Nd} sediment represents material from several primitive sources. Using the isotope proxies alone it is not possible to resolve between these alternatives (i.e., Palawan, Luzon, intra-basin seamounts or volcanic rocks in Borneo).

464

465 *4.2.2 Clay Minerals and Provenance*

466 Clay minerals can also be an aid to provenance because they are partly linked to source as
467 well as environmental conditions. Because climatic variations are known to generate major
468 changes in clay mineralogy, comparable to source rocks compositional differences (Hu et al.,
469 2013) any provenance interpretation based on clays must be compared with other data sets to be
470 considered robust. The effectiveness of clay mineral ratios as provenance proxies can be
471 investigated by comparing clay ratios with ε_{Nd} values. Figure 8A shows the relationship between
472 kaolinite/smectite and ε_{Nd} values. There is a basic correlation between the isotope composition
473 and kaolinite/smectite. This implies that sediment with the most negative ε_{Nd} values tends to
474 have the highest kaolinite/smectite values. This is consistent with the idea that smectite is largely
475 eroded from juvenile volcanic sources, so that abundances of smectite are low when ε_{Nd} values
476 are more negative. The correlation indicates that this clay mineral ratio is largely provenance
477 driven. Likewise, we can examine the provenance dependence of smectite/(illite+chlorite) in
478 Figure 8B. The relationship is less clear in this case, but it is also apparent that the highest values
479 in the clay mineral ratio are only found with the most positive isotopic values, showing some
480 provenance control. Figure 8C shows a good overall correlation between ε_{Nd} values and
481 kaolinite/(illite+chlorite) again indicative of a dominant provenance control on the clay ratio.

482 Smectite is believed to form during the breakdown of volcanic rocks (Hodder et al., 1993)
483 and because we know that there is a significant provenance change prior to ~8 Ma we propose
484 that reduced smectite abundance at that time is probably linked to the reduction in relative input
485 of juvenile volcanic-derived sediment. We use a triangular plot to assess the relative contribution

of chemically weathered kaolinite and smectite compared with physically eroded illite and chlorite. Figure 9 shows that there is a wide range of compositions at the drilling site, but that sediments older than 8 Ma are consistently richer in smectite, while younger sediments trend towards illite and chlorite. Younger sediments tend to plot close to known compositions from the modern Red and Mekong, as well as Taiwan, whereas the older (>8 Ma) sediments approach the composition of sediments sampled offshore Luzon and in rivers draining northern Palawan (Liu et al., 2016). Although some samples younger than 8 Ma overlap the Holocene composition of the Pearl River delta many plot with higher illite + chlorite contents and the trend appears to extend towards an end member similar to the Red River but close also to the modern Mekong, for which no pre-modern samples have yet been measured. The modern Mekong River field is likely displaced towards higher kaolinite contents compared to its older composition as a result of agriculture in the basin, as noted in the Pearl River (Hu et al., 2013).

The clay mineral data argue strongly against significant sediment delivery from arc sources in Sumatra or the Malay Peninsula, or from volcanic sources in Borneo. However, the progressive development of a more physically eroded illite and chlorite-rich assemblage is consistent with a shift in provenance from juvenile volcanic sources to more continental influence.

We further explore the potential use of clay minerals to determine sediment provenance by consideration of the illite chemistry index (Petschick et al., 1996), together with the ratio kaolinite/(illite+chlorite), following the study of Hu et al. (2014). Figure 10 shows that the sediments at Site U1433 comprise a relatively restricted range, largely lying within the physical weathering regime, with moderate degrees of hydrolysis due to chemical weathering. They are most similar to the average composition of sediments from northern Borneo, and the Red and

509 Mekong Rivers but contrast with strongly chemically weathered sediments Hainan Island, as
510 well as the Pearl River. Such a pattern is consistent with our earlier provenance conclusions
511 emphasizing flux from Indochina after 8 Ma and ruling out significant sources in southern China
512 or Hainan. Modern rivers in the Malay Peninsular and Sumatra have kaolinite/(illite+chlorite)
513 values >3.5 and are clearly excluded (Liu et al., 2012).

514 The highest illite chemical index values appear to be associated with sediments older than
515 8 Ma, and there is relative stability in illite chemistry and illite crystallinity indices in sediments
516 younger than 8 Ma. Sediment appears to be largely derived from areas experiencing strong
517 physical erosion and would be consistent with much of the sediment coming from the Mekong
518 and associated rivers draining Indochina since 8 Ma. The Mekong derives most of its sediment
519 load from its headwaters in SE Tibet (Clift et al., 2006b). The Pearl River is not a good match
520 based on these proxies. The clay mineral compositions argue against major derivation of
521 sediment from southern Borneo at any time since 17 Ma.

522

523 *4.3 Mekong River Flux to South China Sea*

524 We argue that most of the sediments at Site U1433 have been derived from the Mekong
525 River since 8 Ma, with lesser input from other small rivers in Vietnam. Between 8 and 4 Ma
526 there is slightly more Sr isotopic difference between the sediments and the modern Mekong
527 River compared to after 4 Ma, and this may reflect either a change in the average composition of
528 that river since that time, or possibly additional flux from more continental sources directly from
529 the coast of Indochina. Nonetheless, the change at 4 Ma is modest, compared to that at 8 Ma.
530 Relative isotopic stability since 8 Ma argues that the Mekong River has been the primary

sediment source after that time and that therefore the river mouth has been in its present location since then. This is older than other seismically derived estimates from the region, which have mostly placed the time of initiation of the Mekong in the present position at around 5 Ma or younger (Li et al., 2013; Murray and Dorobek, 2004). Our data are compatible with this earlier interpretation because our distal location means that Site U1433 might be receiving muddy sediment in plumes from the river mouth at an early stage after the establishment of the mouth in its present location but before the delta clinoforms had migrated into the shelf edge areas covered by the seismic surveys. Regional sediment budgets for this area (Ding et al., 2016) show a sharp increase in sedimentation rates at around this time, consistent with the Mekong either initiating or moving its mouth to the present location around this time. Although the age of the Mekong in the SW South China Sea is much younger than many of the other large rivers in SE Asia (Clift et al., 2006a; Robinson et al., 2013; Zheng et al., 2013) our data does not preclude the existence of an older Mekong River, probably in the Gulf of Thailand, but would only argue for it moving its mouth to the present location in the Late Miocene.

Although there is evidence for accelerated uplift in SE Tibet-SW China, in the headwaters of the Mekong after ~9–13 Ma (Clark et al., 2005) uplift in that area began much earlier (Wang et al., 2012), so that it seems unlikely that the plateau uplift triggered the move of the Mekong mouth to the present location at around 8 Ma. The fact that the Yangtze, Irrawaddy and Red Rivers have much older histories, but are also sourced from eastern Tibet, further supports the idea that accelerated Late Miocene uplift did not cause the Mekong River to initiate and implies that the change we observe is linked to avulsion of the lower reaches.

It is not apparent why the Mekong River would move its mouth from an earlier location in the Gulf of Thailand (Fig. 1), leaving the modern Chao Phraya as a vestige of its former

554 course. It is possible that this is linked to the uplift of the Central Highlands of Vietnam at
555 around this time (Carter et al., 2000). However, it is noteworthy that the Gulf of Thailand itself
556 shows reduced sedimentation after this time (Clift, 2006) when sediment input to the SW South
557 China Sea increased (Ding et al., 2016). It is possible that the basins in the Gulf of Thailand had
558 been largely filled at that point and that the lack of accommodation space caused the river mouth
559 to avulse towards the southeast from its earlier location.

560 The geochemical and mineralogical history we reconstruct at Site U1433 is markedly
561 different from that recorded on the northern margin of South China Sea adjacent to mainland
562 China. Since both areas share a similar monsoonal climate we would argue that these differences
563 are largely related to changes in sediment provenance. Figure 11 compares records of
564 kaolinite/illite from IODP Site U1433, as well as from ODP Site 1146 on the northern margin
565 and ODP Site 1143 in the Dangerous Grounds, whose clastic sediment has been inferred to come
566 from the Mekong (Wan et al., 2006). Kaolinite/illite is typically linked to the degree of chemical
567 weathering, yet there is no correlation between the record on the northern margin and at Site
568 U1433. The northern margin data show a general decrease in chemical weathering intensity from
569 8 Ma to the present day, correlating with the increasingly cold conditions related to global
570 environmental degradation over that same time (Clift et al., 2014). In contrast, kaolinite/illite at
571 Site U1433 shows a cyclicity through time, closely mirroring the record at ODP Site 1143 (Fig.
572 11). We argue that this correlation with ODP Site 1143, but not with the northern margin,
573 represents a change in the sediment provenance linked to the Mekong River in the SW basin.
574 Indeed the fact that kaolinite/illite values at ODP Site 1143 and IODP Site U1433 not only track
575 each other but are of the same value indicates that they share a common source, i.e., the Mekong.
576 Unfortunately clay mineral analysis of sediment at ODP Site 1143 has not addressed sediment

older than 8.5 Ma, which allows us only to compare the records after the onset of Mekong sediment delivery to the SW South China Sea.

5. Conclusions

We applied a series of geochemical and mineral proxies to the study of sediment from IODP Site U1433 in the SW South China Sea. The objective of our study was to use sedimentary records to reconstruct evolving tectonic and erosional conditions since around 17 Ma. We exploited the tectonic diversity in Southeast Asia, which allows us to resolve sediment eroded from different sources blocks using a matrix of different proxies. Our results show significant temporal variation in the composition of sediment reaching the drilling site with a particularly large change at ~8 Ma. Prior to 8 Ma we see substantial variation in the intensity of chemical alteration, as well as in Sr and Nd isotope characteristics that suggest significant variability of sediment sources at 8–17 Ma. In sediments younger than 8 Ma there is greater stability, with compositions lying relatively close to that of the modern Mekong River. Attempts to use proxies such as the CIA or clay minerals to examine the evolving state of chemical weathering proved to be unsuccessful because the degree of alteration is largely controlled by the provenance and quartz content of the sediment.

The source of sediment can be best constrained by looking at the Sr and Nd isotope characteristics of the clastic fraction. This shows that sediments predating 8 Ma tend to be eroding from more primitive, juvenile crust, but still dominated by a flux of sediment from mainland Indochina. A number of possible volcanic sources were identified, although we favor erosion from Palawan where the ophiolite was already exposed prior to 17 Ma and where the

sediment transport path downslope is clear. Elevated Ni/Zr values before 10 Ma also argue for some flux from a source of this variety. We do not exclude some additional flux from the Luzon arc, although paleogeography and modern current activity suggest that this is not significant. Borneo was located too far to the south to be a significant source before 8 Ma and the known clay mineral assemblage is also inconsistent.

Clay mineral assemblages show that the sediment older than 8 Ma is substantially dominated by smectite, again reflecting the more volcanic juvenile sources of that earlier time. After that time we see an evolution towards clays that are more dominated by illite and chlorite, indicative of stronger physical erosion. Sediments younger than 8 Ma have compositions close to those of the modern Mekong River, which is presumed to dominate the sediment supply. Just as the geochemistry was largely controlled by quartz content (and provenance) so also the clay mineral composition appears to be largely a function of these factors rather than reflecting environmental conditions at the time of sedimentation.

Our records show significant differences in the geochemical and mineral history between SW South China Sea and the northern margin. We learn little about long-term variation in monsoon intensity from this record, but the significant change in provenance especially around 8 Ma is indicative of a start to the Mekong River in its present location. Modern differences between the Mekong and sediments deposited between 8 and 5 Ma thus may reflect either evolution in the Mekong River itself, or more likely additional input from other smaller rivers draining coastal Indochina at that time. An 8 Ma initiation of the Mekong River in the present location is consistent with seismic data but does not require the river to be that young, only to have experienced avulsion of its mouth out of the Gulf of Thailand at that time.

621

622 *Acknowledgments*

623 This research used samples and/or data provided by the International Ocean Discovery Program
624 (IODP). Funding for this research was provided by U.S. Science Support Program and the
625 Charles T. McCord chair in petroleum geology at Louisiana State University. Portions of this
626 material are based upon work supported while RWM was serving at the National Science
627 Foundation. The manuscript has been improved thanks to comments from two anonymous
628 reviewers.

629

Figure Captions

Figure 1. Bathymetric map of the South China Sea indicates the location of IODP Site U1433 that is the subject of this study. Topography is from Shuttle Radar Topography Mission (SRTM) plotted by GeoMapApp. Major fluvial systems which deliver sediments into the South China Sea are also shown, together with the Molengraaff River of glacial age crossing the Sunda Shelf (Molengraaff and Weber, 1919). Yellow arrows show surface currents active during summer monsoon (Fang et al., 1998). Isobaths are shown in 1000 m intervals. Vietnamese Central Highlands = VCH. SG = Song Gianh.

Figure 2. Geochemical variations at IODP Site U1433 plotted against depth. There is a trend towards lower CIA above ~250 msbf above the zone of frequent calcareous turbidites. Note that both Nd and Sr isotopes show a two stage trend with a break at 700 mbsf. Uncertainties for Nd are the external reproducibility. Those in Sr isotopes are within the size of the plotted symbol. LSR = linear sedimentation rate. Uncertainties in Sr isotope composition are within the size of the plotted symbols. Sedimentation rates are calculated from shipboard magnetic and biostratigraphic constraints (Li et al., 2015), with no sediment compaction correction.

Figure 3. Geochemical and mineralogical proxies for weathering intensity and provenance at IODP Site U1433. Sediment flux for the Mekong delta derived from regional seismic data is from Clift (2006). Uncertainties in the isotope ratios are smaller than the symbols plotted. Horizontal gray bars show periods of anomalous high ε_{Nd} values, suggestive of a different provenance. DRU = Deep Regional Unconformity of Hutchison (2005). “Seismic delta” represents the time of the oldest foresets of the Mekong delta identified by Li et al. (2013). Uncertainties in Sr isotope composition are within the size of the plotted symbols. CIA and kaolinite/(illite+chlorite) are shown with raw data in gray and a 5-point running average in black drawn to emphasize the long term changes. Sealevel curve is from Haq et al. (1987).

Figure 4. Comparison of temporal evolution in the sand content as proxied by (A) Si/Al compared to (B) chemical index of alteration (CIA). Note that strong similarity between the two proxies suggestive of a major quartz silt-sand control on chemical weathering intensity. Five point running average is used to show the long wavelength variation which makes the parallel evolution easier to appreciate.

Figure 5. Trace element discrimination diagrams to determine tectonic setting. (A) Cr/V versus Y/Ni from Hiscott (1984). PAAS = post-Archean Australian shale, UCC = Upper Continental Crust (Taylor and McLennan, 1985), and (B) TiO_2 versus Zr concentrations from Nagarajan et al. (2014).

Figure 6. Plot of Sr versus Nd isotopes for the samples from IODP Site U1433 broken into four separate age populations and compared with potential source bedrock compositions and other known sediment compositions from the region. Annamite Range river is from Jonell et al. (2016), Red and Mekong River is from Liu et al. (2007), offshore Borneo, Dangerous Grounds sediment data are from Wei et al. (2012), Palawan is from Tu et al. (1992), Sumatra data is from White and Patchett (1984). Luzon data is from Knittel et al. (1988). Hainan bedrock data is from Fang et al. (1992). Taiwan River data is from Chen and Lee (1990) and Lan et al. (2002). Pearl River data is from Hu et al. (2013). Stars show mixing end members with the curves showing possible compositions between these sources. Indochina end member has Sr and Nd concentrations of 120 and 40.1 ppm respectively from Liu et al. (2007) measurements of the Red and Mekong Rivers. The Palawan end member has Sr and Nd concentrations of 542 and 19 ppm from Tu et al. (1992). The Luzon arc end member has Sr and Nd concentrations of 439 and 19.1 ppm respectively, averaged Luzon data from Georoc.

Figure 7. Paleogeographic map of the South China Sea at 8 Ma and 17 Ma. Luzon and the Philippine arc have been moving from the Pacific towards the South China Sea progressively over this interval. Note emergence of Borneo prior to 8 Ma and the emplacement of the Central Highlands (CH) lavas at 8 Ma. Map modified from Hall (2002).

Figure 8. Plots of ε_{Nd} values and select clay mineral ratios show some correlation between provenance and clay mineral assemblage. (A) Smectite/kaolinite versus ε_{Nd} values indicates more smectite in sediments with more primitive provenance (higher ε_{Nd} values). (B) Smectite/(chlorite+illite) shows higher values from samples older than 8 Ma, together with more positive ε_{Nd} values. (C) kaolinite/(illite+chlorite) shows a good overall correlation, but a poor within the 0–4 Ma group.

Figure 9. Ternary diagram of clay minerals from IODP Site U1433 indicates shift in clay mineral assemblage from smectite-dominated to illite and chlorite dominated with younger ages, as shown in Figure 3. Clay mineral data from other fluvial systems are plotted to compare their clay mineral assemblages. Red and Mekong River data are from Liu et al. (2007). Pearl River data are from Hu et al. (2013). Taiwan data is from Liu et al. (2010). West Borneo, Malay Peninsula, Sumatra, Luzon data are from Liu et al. (2012). Palawan data is from Liu et al. (2016a).

Figure 10. Correlation of kaolinite/(illite + chlorite) with illite chemical index, showing the different forcing processes on the clay mineral assemblages in the surrounding areas. Figure and Hainan river data are modified from Hu et al. (2014). Pearl, Mekong and Red River points represent averages from Liu et al. (2007). Average Taiwan river data are from Liu et al. (2008). Average Borneo river data are from Liu et al. (2012)

Figure 11. Temporal evolution in kaolinite/illite at Site IODP U1433 compared to similar data from the northern margin of South China Sea at ODP Site 1146 (Wan et al., 2007) and in the SW, Dangerous Grounds at ODP Site 1143 (Wan et al., 2006). Chemical weathering is compared with global compilation of the Zachos et al. (2001).

Table 1. Major element composition of sediments derived by ICP-ES.

Table 2. Strontium and neodymium isotope compositions. External precision of the $^{87}Sr/^{86}Sr$ and $^{143}Nd/^{144}Nd$ measurements is estimated to be 0.000015–0.000025 (2σ) and 0.000010–0.000020 (2σ) respectively.

Table 3. Calculated clay mineral assemblages derived from XRD analysis.

Table S1. Major and trace element composition of replicate analyses and standards.

6. References

Andrews, J.E., Brimblecombe, P., Jickells, T.D., Liss, P.S., Reid, B., 2013. An Introduction to Environmental Chemistry. John Wiley & Sons, New York, 320 pp.

Aurelio, M.A., Forbes, M.T., Taguibao, K.J.L. et al., 2013. Middle to Late Cenozoic tectonic events in south and central Palawan (Philippines) and their implications to the evolution of the south- eastern margin of South China Sea: Evidence from onshore structural and offshore seismic data. Marine and Petroleum Geology. doi:10.1016/j.marpetgeo.2013.12.002.

Barckhausen, U., Engels, M., Franke, D., Ladage, S., Pubellier, M., 2014. Evolution of the South China Sea: Revised ages for breakup and seafloor spreading. Marine and Petroleum Geology. doi:10.1016/j.marpetgeo.2014.02.022.

Birkeland, P.W., 1984. Soils and geomorphology. Oxford University Press, Oxford, 310 pp.

Biscaye, P.E., 1965. Mineralogy and sedimentation of recent deep-sea clay in the Atlantic Ocean and adjacent seas and oceans. Geological Society of America Bulletin, 76: 803–832.

Boulay, S., Colin, C., Trentesaux, A., Clain, S., Liu, Z., Lauer-Leredde, C., 2007. Sedimentary responses to the Pleistocene climatic variations recorded in the South China Sea. Quaternary Research, 68: 162–172.

Briais, A., Patriat, P., Tapponnier, P., 1993. Updated interpretation of magnetic anomalies and seafloor spreading stages in the South China Sea: implications for the Tertiary tectonics of Southeast Asia. Journal of Geophysical Research, 98: 6299-6328. doi:10.1029/92JB02280.

Burbank, D.W., Blythe, A.E., Putkonen, J., Pratt-Sitaula, B., Gabet, E., Oskins, M., Barros, A., Ojha, T.P., 2003. Decoupling of erosion and precipitation in the Himalayas. Nature, 426: 652–655.

Carter, A., Roques, D., Bristow, C., Kinny, P.D., 2001. Understanding Mesozoic accretion in Southeast Asia: Significance of Triassic thermotectonism (Indosinian orogeny) in Vietnam. Geology, 29: 211–214.

Carter, A., Roques, D., Bristow, C.S., 2000. Denudation history of onshore central Vietnam: constraints on the Cenozoic evolution of the western margin of the South China Sea. Tectonophysics, 322: 265–277.

Chen, C.H., Lee, T., 1990. A Nd-Sr isotopic study on river sediments of Taiwan. Proceedings of the Geological Society of China, 33(4): 339-350.

Chu, P.C., Li, R., 2000. South China Sea Isopycnal-Surface Circulation. Journal of Physical Oceanography, 30: 2419–2438.

Clark, M.K., House, M.A., Royden, L.H., Whipple, K.X., Burchfiel, B.C., Zhang, X., Tang, W., 2005. Late Cenozoic uplift of southeastern Tibet. Geology, 33(6): 525-528. doi: 10.1130/G21265.1.

Clark, M.K., Schoenbohm, L.M., Royden, L.H., Whipple, K.X., Burchfiel, B.C., Zhang, X., Tang, W., Wang, E., Chen, L., 2004. Surface uplift, tectonics, and erosion of eastern Tibet from large-scale drainage patterns. Tectonics, 23, TC1006. doi:10.1029/2002TC001402.

Clift, P.D., 2006. Controls on the erosion of Cenozoic Asia and the flux of clastic sediment to the ocean. Earth and Planetary Science Letters, 241(3-4): 571-580.

765 Clift, P.D., 2015. Assessing effective provenance methods for fluvial sediment in the South
766 China Sea. In: Clift, P.D., Harff, J., Wu, J., Yan, Q. (Eds.), River-dominated shelf
767 sediments of East Asian seeds, 429, Geological Society, London, doi:10.1144/SP429.3.
768 Clift, P.D., Blusztajn, J., Nguyen, D.A., 2006a. Large-scale drainage capture and surface uplift in
769 eastern Tibet-SW China before 24 Ma inferred from sediments of the Hanoi Basin,
770 Vietnam. Geophysical Research Letters, 33(L19403). doi:10.1029/2006GL027772.
771 Clift, P.D., Carter, A., Campbell, I.H., Pringle, M., Hodges, K.V., Lap, N.V., Allen, C.M., 2006b.
772 Thermochronology of mineral grains in the Song Hong and Mekong Rivers, Vietnam.
773 Geophysics, Geochemistry, Geosystems, 7(Q10005). doi:10.1029/2006GC001336.
774 Clift, P.D., Lee, G.H., Nguyen, A.D., Barckhausen, U., Hoang, V.L., Sun, Z., 2008. Seismic
775 evidence for a Dangerous Grounds mini-plate: No extrusion origin for the South China
776 Sea. Tectonics, 27(TC3008). doi:10.1029/2007TC002216.
777 Clift, P.D., Vannucchi, P., Phipps Morgan, J., 2009. Crustal redistribution, crust-mantle
778 recycling and Phanerozoic evolution of the continental crust. Earth Science Reviews, 97:
779 80-104. doi:10.1016/j.earscirev.2009.10.003.
780 Clift, P.D., Wan, S., Blusztajn, J., 2014. Reconstructing Chemical Weathering, Physical Erosion
781 and Monsoon Intensity since 25 Ma in the northern South China Sea: A review of
782 competing proxies. Earth-Science Reviews, 130: 86-102.
783 doi:10.1016/j.earscirev.2014.01.002.
784 Colin, C., Siani, G., Sicre, M.-A., Liu, Z., 2010. Impact of the East Asian monsoon rainfall
785 changes on the erosion of the Mekong River basin over the past 25,000 yr. Marine
786 Geology, 271(1-2): 84-92. doi:10.1016/j.margeo.2010.01.013.
787 Cullen, A., Reemst, P., Henstra, G., Gozzard, S., Ray, A., 2010. Rifting of the South China Sea:
788 new perspectives. Petroleum Geoscience, 16: 273–282.
789 Cung, T.C., Dorobek, S., Richter, C., Flower, M., Kikawa, E., Nguyen, Y.T., McCabe, R., 1998.
790 Paleomagnetism of Late Neogene basalts in Vietnam and Thailand: Implications for the
791 post-Miocene tectonic history of Indochina. In: Flower, M.F.J., Chung, S.-L., Lo, C.-H.,
792 Lee, T.Y. (Eds.), Mantle Dynamics and Plate Interactions in East Asia. Geodynamic
793 Series, 27, American Geophysical Union, Washington, D.C., pp. 289-299,
794 Deniel, C., Pin, C., 2001. Single-stage method for the simultaneous isolation of lead and
795 strontium from silicate samples for isotopic measurements. Analytica Chimica Acta,
796 426(1): 95-103.
797 DePaolo, D.J., Wasserburg, G.J., 1976. Nd isotopic variations and petrogenetic models.
798 Geophysical Research Letters, 3(5): 249-252.
799 Ding, W., Li, J., Clift, P.D., IODP Expedition 349 Scientists, 2016. Spreading dynamics and
800 sedimentary process of the Southwest Sub-basin, South China Sea: Constraints from
801 multi-channel seismic data and IODP Expedition 349. Journal of Asian Earth Sciences,
802 115(1): 97-113. doi:10.1016/j.jseaes.2015.09.013.
803 Edzwald, J.K., O'Melia, C.R., 1975. Clay distributions in recent estuarine sediments. Clays and
804 Clay Minerals, 23: 39-44.
805 Fang, G., Fang, W., Fang, Y., Wang, K., 1998. A survey of studies on the South China Sea upper
806 ocean circulation. Acta Oceanography of Taiwanica, 37(1): 1–16.
807 Fang, Z., Zhao, J.-X., McCulloch, M.T., 1992. Geochemical and Nd isotopic study of Palaeozoic
808 bimodal volcanics in Hainan Island, South China—Implications for rifting tectonics and
809 mantle reservoirs. Lithos, 29(1–2): 127–139. doi:10.1016/0024-4937(92)90037-Y.

Fletcher, C.J.N., Chan, L.S., Sewell, R.J., Campbell, S.D.G., Davis, D.W., Zhu, J., 2004. Basement heterogeneity in the Cathaysia crustal block, southeast China. In: Malpas, J., Fletcher, C.J.N., Ali, J.R., Aitchison, J.C. (Eds.), Aspects of the Tectonic Evolution of China. Special Publication, 226, Geological Society, London, pp. 145-155, doi:10.1144/GSL.SP.2004.226.01.08.

Garçon, M., Chauvel, C., France-Lanord, C., Huyghe, P., Lavé, J., 2013. Continental sedimentary processes decouple Nd and Hf isotopes. Geochimica et Cosmochimica Acta, 121: 177-195. doi:doi.org/10.1016/j.gca.2013.07.027.

Garçon, M., Chauvel, C., France-Lanord, C., Limonta, M., Garzanti, E., 2014. Which minerals control the Nd–Hf–Sr–Pb isotopic compositions of river sediments? Chemical Geology, 364: 42–55. doi:10.1016/j.chemgeo.2013.11.018.

Gibbs, R.J., 1977. Clay mineral segregation in the marine environment. Journal of Sediment Petrology, 47: 237-243.

Hall, R., 2002. Cenozoic geological and plate tectonic evolution of SE Asia and the SW Pacific: computer-based reconstructions and animations. Journal of Asian Earth Sciences, 20: 353-434.

Hamilton, P.J., O'Nions, R.K., Bridgwater, D., Nutman, A., 1983. Sm-Nd Studies of Archean Metasediments and Metavolcanics from West Greenland and Their Implications for the Earths Early History. Earth and Planetary Science Letters, 62(2): 263-272.

Haq, B.U., Hardenbol, J., Vail, P.R., 1987. Chronology of fluctuating sea levels since the Triassic. Science, 235: 1156–1167.

Hayes, D.E., Lewis, S.D., 1984. A geophysical study of the Manila Trench, Luzon, Philippines; 1, Crustal structure, gravity, and regional tectonic evolution. Journal of Geophysical Research, 89: 9171–9195.

Hillier, S., 1995. Erosion, sedimentation, and sedimentary origin of clays. In: Velde, B. (Ed.), Clays and the environment, Springer Verlag, Berlin, pp. 162-219,

Hinz, K., Fritsch, J., Kempter, E.H.K., Mohammad, A.M., Meyer, J., Mohamed, D., Vosberg, H., Weber, J., Benavidez, J., 1989. Thrust tectonics along the north-western continental margin of Sabah/Borneo. Geologische Rundschau, 78(3): 705-730.

Hiscott, R.N., 1984. Ophiolitic source rocks for Taconic-age flysch: trace element evidence. Geological Society of America Bulletin, 95, : 1261–1267.

Hoang, L.V., Wu, F.Y., Clift, P.D., Wysocka, A., Swierczewska, A., 2009. Evaluating the evolution of the Red River system based on in-situ U-Pb dating and Hf isotope analysis of zircons. Geochemistry Geophysics Geosystems, 10(Q11008). doi:10.1029/2009GC002819.

Hoang, N., Flower, M., 1998. Petrogenesis of Cenozoic Basalts from Vietnam: Implication for Origins of a 'Diffuse Igneous Province'. Journal of Petrology, 39(3): 369-395. doi:10.1093/petroj/39.3.369.

Hodder, A.P.W., Naish, T.R., Nelson, C.S., 1993. A two-stage model for the formation of smectite from detrital volcanic glass under shallow-marine conditions. Marine Geology, 109(3–4): 279–285. doi:10.1016/0025-3227(93)90066-5.

Honza, E., John, J., Banda, R.M., 2000. An imbrication model for the Rajang accretionary complex in Sarawak, Borneo. Journal of Asian Earth Sciences, 18(6): 751-759.

Hu, B., Li, J., Cui, R. et al., 2014. Clay mineralogy of the riverine sediments of Hainan Island, South China Sea: Implications for weathering and provenance. Journal of Asian Earth Sciences, 96: 84–92. doi:10.1016/j.jseaes.2014.08.036.

Hu, D., Clift, P.D., Böning, P., Hannigan, R., Hillier, S., Blusztajn, J., Wang, S., Fuller, D.Q., 2013. Holocene evolution in weathering and erosion patterns in the Pearl River delta. Geochemistry Geophysics Geosystems, 14. doi:10.1002/ggge.20166.

Hutchison, C.S., 2004. Marginal basin evolution; the southern South China Sea. Marine and Petroleum Geology, 21(9): 1129-1148. doi:10.1016/j.marpetgeo.2004.07.002.

Hutchison, C.S., 2005. Geology of North-West Borneo: Sarawak, Brunei and Sabah. Elsevier, Amsterdam, 448 pp.

Hutchison, C.S., Vijayan, V.R., 2010. What are the Spratly Islands? Journal of Asian Earth Sciences, 39(5): 371-385. doi:10.1016/ j.jseaes.2010.04.013.

Jahn, B.M., Zhou, X.H., Li, J.L., 1990. Formation and tectonic evolution of Southeastern China and Taiwan: Isotopic and geochemical constraints. Tectonophysics, 183: 145-160.

Jonell, T.N., Clift, P.D., Hoang, L.V., Hoang, T., Carter, A., Wittmann, H., Böning, P., Pahnke, K., Rittenour, T., 2016. Controls on Erosion Patterns and Sediment Transport in a Monsoonal, Tectonically Quiescent Drainage, Song Gianh, Central Vietnam. Basin Research: 1-25. doi: 10.1111/bre.12199.

Knittel, U., Defant, M.J., Raczek, I., 1988. Recent enrichment in the source region of arc magmas from Luzon island, Philippines: Sr and Nd isotopic evidence. Geology, 16(1): 73-76. doi: 10.1130/0091-7613(1988)016.

Lan, C.Y., Lee, C.-S., Shen, J.J.-S., Lu, C.Y., Mertzman, S.A., Wu, T.-W., 2002. Nd -Sr isotopic composition and geochemistry of sediments from Taiwan and their implications. Western Pacific Earth Sciences, 2(2): 205-222.

Lavé, J., Avouac, J.P., 2001. Fluvial incision and tectonic uplift across the Himalaya of central Nepal. Journal of Geophysical Research, 106: 26,561–26,592. doi: 10.1029/2001JB000359.

Lepvrier, C., Maluski, H., Vu, V.T., Leyreloup, A., Phan, T.T., Vuong, N.V., 2004. The Early Triassic Indosinian orogeny in Vietnam (Truong Son Belt and Kontum Massif); implications for the geodynamic evolution of Indochina. Tectonophysics, 393: 87-118. doi:10.1016/j.tecto.2004.07.030.

Li, C.-F., Lin, J., Kulhanek, D.K. et al., 2015. Site U1433. Proceedings of the International Ocean Discovery Program, 349. doi:10.14379/iodp.proc.349.105.2015.

Li, C.-F., Xu, X., Expedition 349 Scientific Party, 2014. Ages and magnetic structures of the South China Sea constrained by deep tow magnetic surveys and IODP Expedition 349. Geochemistry, Geophysics, Geosystems, 15: 4958–4983. doi:10.1002/ 2014GC005567.

Li, L., Clift, P.D., Nguyen, H.T., 2013. The sedimentary, magmatic and tectonic evolution of the Southwestern South China Sea revealed by seismic stratigraphic analysis. Marine Geophysical Research, 34: 393–406. doi:10.1007/s11001-013-9171-y.

Liu, J.P., Xue, Z., Ross, K., H, J.W., Yang, Z.S., Li, A.C., Gao, S., 2009a. Fate of sediments delivered to the sea by Asian large rivers: Long-distance transport and formation of remote alongshore clinothems. The Sedimentary Record, 7(4): 4-9.

Liu, Z., Colin, C., Huang, W., Le, K.P., Tong, S., Chen, Z., Trentesaux, A., 2007. Climatic and tectonic controls on weathering in south China and Indochina Peninsula: Clay mineralogical and geochemical investigations from the Pearl, Red, and Mekong drainage basins. Geochemistry Geophysics Geosystems, 8, Q05005. doi:10.1029/2006GC001490.

Liu, Z., Colin, C., Li, X. et al., 2010. Clay mineral distribution in surface sediments of the northeastern South China Sea and surrounding fluvial drainage basins: Source and transport. Marine Geology, 277: 48–60. doi:10.1016/j.margeo.2010.08.010.

902 Liu, Z., Colin, C., Trentesaux, A., Siani, G., Frank, N., Blamart, D., Farid, S., 2005. Late
903 Quaternary climatic control on erosion and weathering in the eastern Tibetan Plateau and
904 the Mekong Basin. Quaternary Research, 63: 316-328.
905 Liu, Z., Tuo, S., Colin, C. et al., 2008. Detrital fine-grained sediment contribution from Taiwan
906 to the northern South China Sea and its relation to regional ocean circulation. Marine
907 Geology, 255(3-4): 149-155.
908 Liu, Z., Wang, H., Hantoro, W.S., Sathiamurthy, E., Colin, C., Zhao, Y., Li, J., 2012. Climatic
909 and tectonic controls on chemical weathering in tropical Southeast Asia (Malay Peninsula,
910 Borneo, and Sumatra). Chemical Geology, 291: 1-12.
911 Liu, Z., Zhao, Y., Colin, C., Siringan, F.P., Wu, Q., 2009b. Chemical weathering in Luzon,
912 Philippines from clay mineralogy and major-element geochemistry of river sediments.
913 Applied Geochemistry, 24: 2195–2205.
914 Liu, Z., Zhao, Y., Colin, C. et al., 2016a. Source-to-sink transport processes of fluvial sediments
915 in the South China Sea. in press. doi:10.1016/j.earscirev.2015.08.005.
916 Liu, Z., Zhao, Y., Colin, C. et al., 2016b. Source-to-sink transport processes of fluvial sediments
917 in the South China Sea. Earth Science Reviews, 153: 238-273.
918 doi:10.1016/j.earscirev.2015.08.005.
919 Lupker, M., France- Lanord, C., Lavé, J., Bouchez, J., Galy, V., Métivier, F., Gaillardet, J.,
920 Lartiges, B., Mugnier, J.L., 2011. A Rouse- based method to integrate the chemical
921 composition of river sediments: Application to the Ganga basin. Journal of Geophysical
922 Research, 116(F04012). doi:10.1029/2010JF001947.
923 McLennan, S.M., 1993. Weathering and global denudation. The Journal of Geology, 101: 295–
924 303.
925 Metcalfe, I., 1996. Pre-Cretaceous evolution of SE Asian terranes. In: Hall, R., Blundell, D.J.
926 (Eds.), Tectonic evolution of SE Asia. Special Publication, 106, Geological Society
927 London, pp. 97–122,
928 Métivier, F., Gaudemer, Y., Tapponnier, P., Klein, M., 1999. Mass accumulation rates in Asia
929 during the Cenozoic. Geophysical Journal International, 137(2): 280-318.
930 Mielke, J.E., 1979. Composition of the Earth's crust and distribution of the elements. In: Siegel,
931 F.R. (Ed.), Review of Research on Modern Problems in Geochemistry, UNESCO, Paris,
932 pp. 13-36,
933 Milliman, J.D., Farnsworth, K.L., 2011. River Discharge to the Coastal Ocean: a Global
934 Synthesis, 384. Cambridge University Press, Cambridge.
935 Milliman, J.D., Farnsworth, K.L., Albertin, C.S., 1999. Flux and fate of fluvial sediments leaving
936 large islands in the East Indies. Journal of Sea Research, 41(1–2): 97-107.
937 Milliman, J.D., Syvitski, J.P.M., 1992. Geomorphic/tectonic control of sediment discharge to the
938 ocean; the importance of small mountainous rivers. Journal of Geology, 100: 525-544.
939 Molengraaff, G.A.E., Weber, M., 1919. Het verband tusschen den plistoceenen ijstijd en het
940 ontstaan der Soenda-zee (Java- en Zuid-Chmeesche Zee) en de invloed daarvan op de
941 verspreidmg der koraalriffen en op de land-en zoetwater-fauna. Verslag Van de Gewone
942 Vergaderingen der Wis-En Natuurkundige Afdeeling, 28: 497-544.
943 Morley, C.K., 2002. A tectonic model for the Tertiary evolution of strike-slip faults and rift
944 basins in SE Asia. Tectonophysics, 347(4): 189-215.
945 Murray, M.R., Dorobek, S.L., 2004. Sediment supply, tectonic subsidence, and basin-filling
946 patterns across the southwestern South China Sea during Pliocene to Recent time. In:
947 Clift, P., Wang, P., Kuhnt, W., Hayes, D. (Eds.), Continent-ocean interactions within east

948 Asian marginal seas. Geophysical Monograph, 149, American Geophysical Union,
949 Washington, DC, pp. 235-254,
950 Nagarajan, R., Roy, P.D., Jonathan, M.P., Lozano, R., Kessler, F.L., Prasanna, M.V., 2014.
951 Geochemistry of Neogene sedimentary rocks from Borneo Basin, East Malaysia:Paleo-
952 weathering, provenance and tectonic setting. Chemie der Erde, 74: 139–146.
953 doi:10.1016/j.chemer.2013.04.003.
954 Nesbitt, H.W., Markovics, G., Price, R.C., 1980. Chemical processes affecting alkalis and
955 alkaline earths during continental weathering. Geochimica et Cosmochimica Acta, 44:
956 1659–1666.
957 Nesbitt, H.W., Young, G.M., 1982. Early Proterozoic climates and plate motions inferred from
958 major element chemistry of lutites. Nature, 299(5885): 715-717.
959 Petschick, R., Kuhn, G., Gingele, F., 1996. Clay mineral distribution in surface sediments of the
960 South Atlantic: sources, transport, and relation to oceanography. Marine Geology, 130:
961 203–229.
962 Replumaz, A., Tapponnier, P., 2003. Reconstruction of the deformed collision zone between
963 India and Asia by backward motion of lithospheric blocks. Journal of Geophysical
964 Research, 108, 2285(B6). doi:10.1029/2001JB000661.
965 Riebe, C.S., Kirchner, J.W., Granger, D.E., Finkel, R.C., 2001. Strong tectonic and weak
966 climatic control of long-term chemical weathering rates. Geology, 29: 511-514.
967 Robinson, R.A.J., Brezina, C.A., Parrish, R.R. et al., 2013. Large rivers and orogens: The
968 evolution of the Yarlung Tsangpo–Irrawaddy system and the eastern Himalayan syntaxis.
969 Gondwana Research. doi:10.1016/j.gr.2013.07.002.
970 Ru, K., Pigott, J.D., 1986. Episodic rifting and subsidence in the South China Sea. AAPG
971 Bulletin, 70(9): 1136–1155.
972 Savva, D., Pubellier, M., Franke, D., Chamot-Rooke, N., Meresse, F., Steuer, S., Auxietre, J.L.,
973 2014. Different expressions of rifting on the South China Seas margins. Marine and
974 Petroleum Geology, 58: 579-598.
975 Shi, X., Kohn, B., Spencer, S., Guo, X., Li, Y., Yang, X., Shi, H., Gleadow, A., 2011. Cenozoic
976 denudation history of southern Hainan Island, South China Sea: Constraints from low
977 temperature thermochronology. Tectonophysics, 504: 100–115.
978 Simons, W., Socquet, A., Vigny, C. et al., 2007. A decade of GPS in Southeast Asia: Resolving
979 Sundaland motion and boundaries. Journal of Geophysical Research, 112(B06420).
980 doi:10.1029/2005JB003868.
981 Singh, S.K., Sarin, M.M., France-Lanord, C., 2005. Chemical erosion in the eastern Himalaya;
982 major ion composition of the Brahmaputra and d13C of dissolved inorganic carbon.
983 Geochimica et Cosmochimica Acta, 69(14): 3573-3588.
984 Su, D., White, N., McKenzie, D., 1989. Extension and subsidence of the Pearl River mouth basin,
985 northern South China Sea. Basin Research, 2: 205–222.
986 Tapponnier, P., Peltzer, G., Le Dain, G., A. Y., Armijo, R., Cobbold, P.R., 1982. Propagating
987 extrusion tectonics in Asia: New insights from simple experiments with plasticine.
988 Geology, 10: 611– 616.
989 Taylor, B., Hayes, D.E., 1983. Origin and history of the South China Sea basin. In: Hayes, D.E.
990 (Ed.), The Tectonic and Geologic Evolution of the Southeast Asian Seas and Islands, 27,
991 American Geophysical Union, Washington, D.C., pp. 23–56,
992 Taylor, S.R., McLennan, S.M., 1985. The continental crust: Its composition and evolution.
993 Blackwell Scientific, Palo Alto, CA, 328 pp.

Thirlwall, M.F., 1991. Long-term reproducibility of multicollector Sr and Nd isotope ratio analysis. Chemical Geology: Isotope Geoscience section, 94(2): 85-104.

Thiry, M., 2000. Palaeoclimatic interpretation of clay minerals in marine deposits; an outlook from the continental origin. Earth-Science Reviews, 49(1-4): 201-221.

Tu, K., Flower, M.F.J., Carlson, R.W., Xie, G., Chen, C.-Y., Zhang, M., 1992. Magmatism in the South China Basin: 1. Isotopic and trace-element evidence for an endogenous Dupal mantle component. Chemical Geology, 97(1–2): 47–63. doi:10.1016/0009-2541(92)90135-R.

Wan, S., Li, A., Clift, P.D., Jiang, H., 2006. Development of the East Asian summer monsoon; evidence from the sediment record in the South China Sea since 8.5 Ma. Palaeogeography, Palaeoclimatology, Palaeoecology, 241: 139-159.

Wan, S., Li, A., Clift, P.D., Stuut, J.-B.W., 2007. Development of the East Asian monsoon: Mineralogical and sedimentologic records in the northern South China Sea since 20 Ma. Palaeogeography, Palaeoclimatology, Palaeoecology, 254(3-4): 561–582.

Wang, E., Kirby, E., Furlong, K.P., Soest, M.v., Xu, G., Shi, X., Kamp, P.J.J., Hodges, K.V., 2012. Two-phase growth of high topography in eastern Tibet during the Cenozoic. Nature Geoscience, 5: 640–645. doi:10.1038/ngeo1538.

Wang, J., Yin, A., Harrison, T.M., Grove, M., Zhang, Y., Xie, G., 2001. A tectonic model for Cenozoic igneous activities in the eastern Indo-Asian collision zone. Earth and Planetary Science Letters, 188(1-2): 123-133.

Wei, G., Liu, Y., Ma, J., Xie, L., Chen, J., Deng, W., Tang, S., 2012. Nd, Sr isotopes and elemental geochemistry of surface sediments from the South China Sea: Implications for Provenance Tracing. Marine Geology, 319–322: 21–34. doi:10.1016/j.margeo.2012.05.007.

White, W.M., Patchett, J., 1984. Hf-Nd-Sr isotopes and incompatible element abundances in island arcs: Implications for magma origins and crust-mantle evolution. Earth and Planetary Science Letters, 67(2): 167–185. doi:10.1016/0012-821X(84)90112-2.

Wobus, C.W., Tucker, G.E., Anderson, R.S., 2010. Does climate change create distinctive patterns of landscape incision? Journal of Geophysical Research, 115(F04008). doi:10.1029/2009JF001562.

Zachos, J., Pagani, M., Sloan, L., Thomas, E., Billups, K., 2001. Trends, rythms and abberations in global climate 65 Ma to Present. Science, 292: 686–693.

Zheng, H., Clift, P.D., Tada, R., Jia, J.T., He, M.Y., Wang, P., 2013. A Pre-Miocene Birth to the Yangtze River. Proceedings of the National Academy of Sciences: 1-6. doi:10.1073/pnas.1216241110.

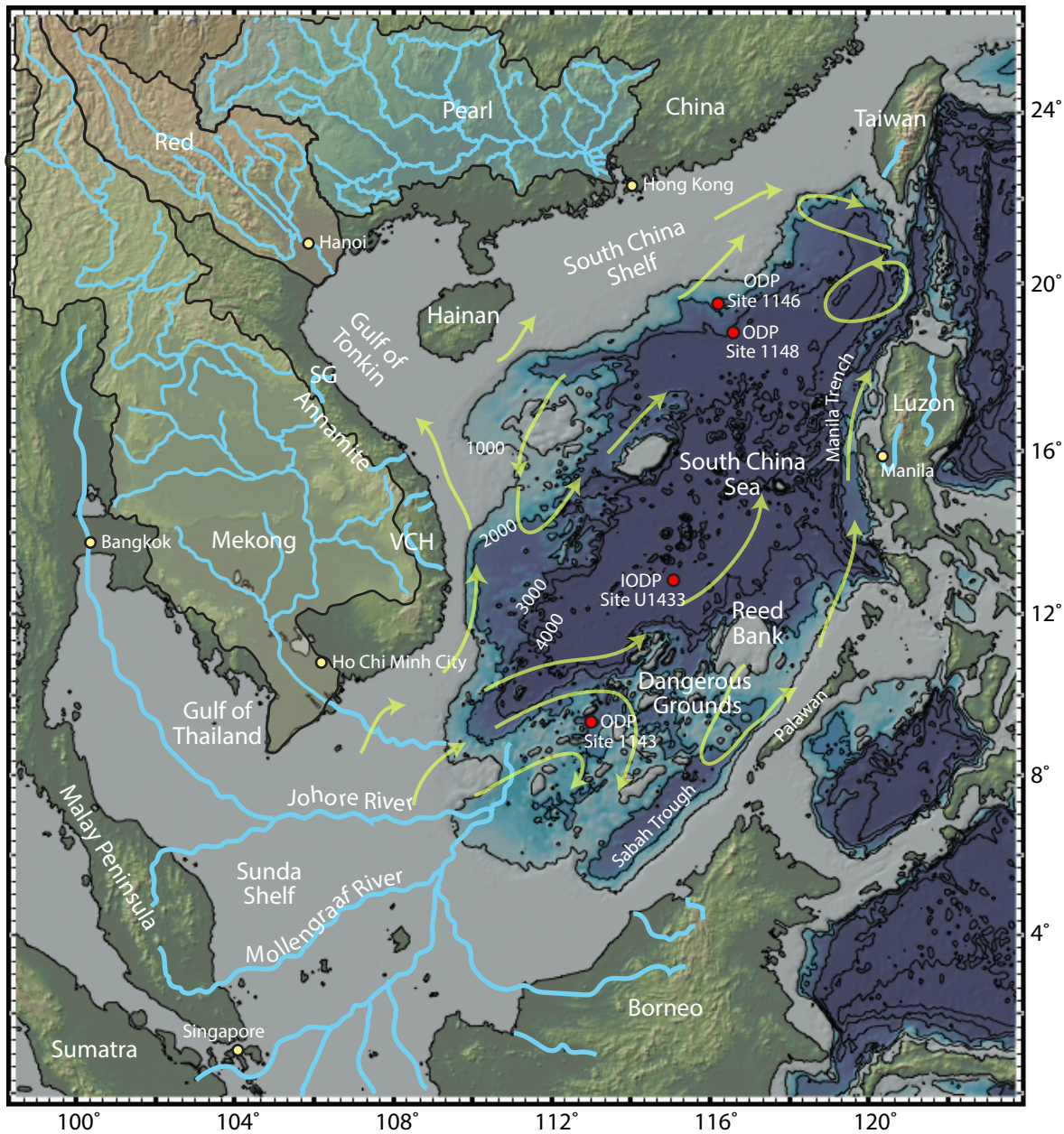

Figure 1
Liu et al.

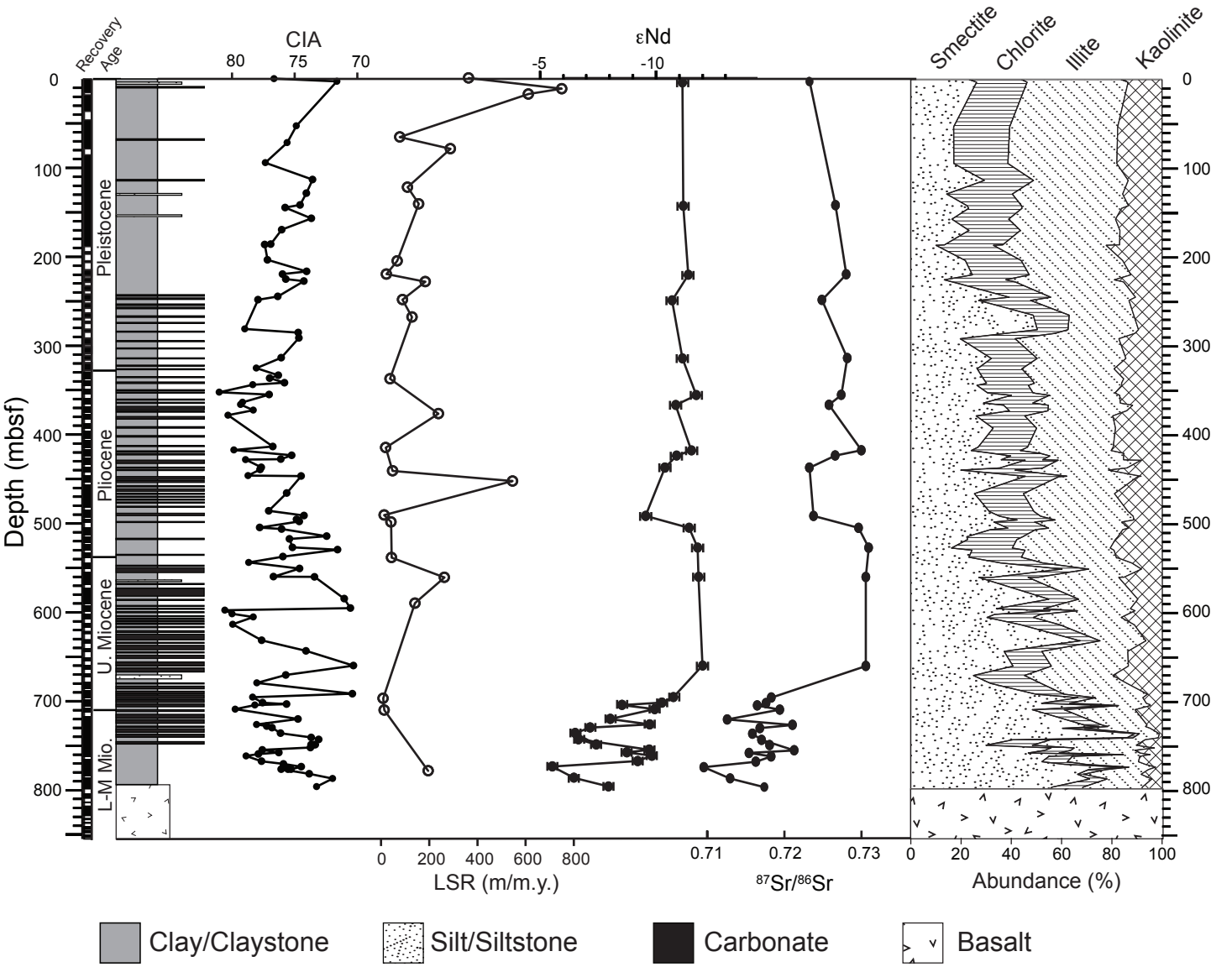

Figure 2
Liu et al.

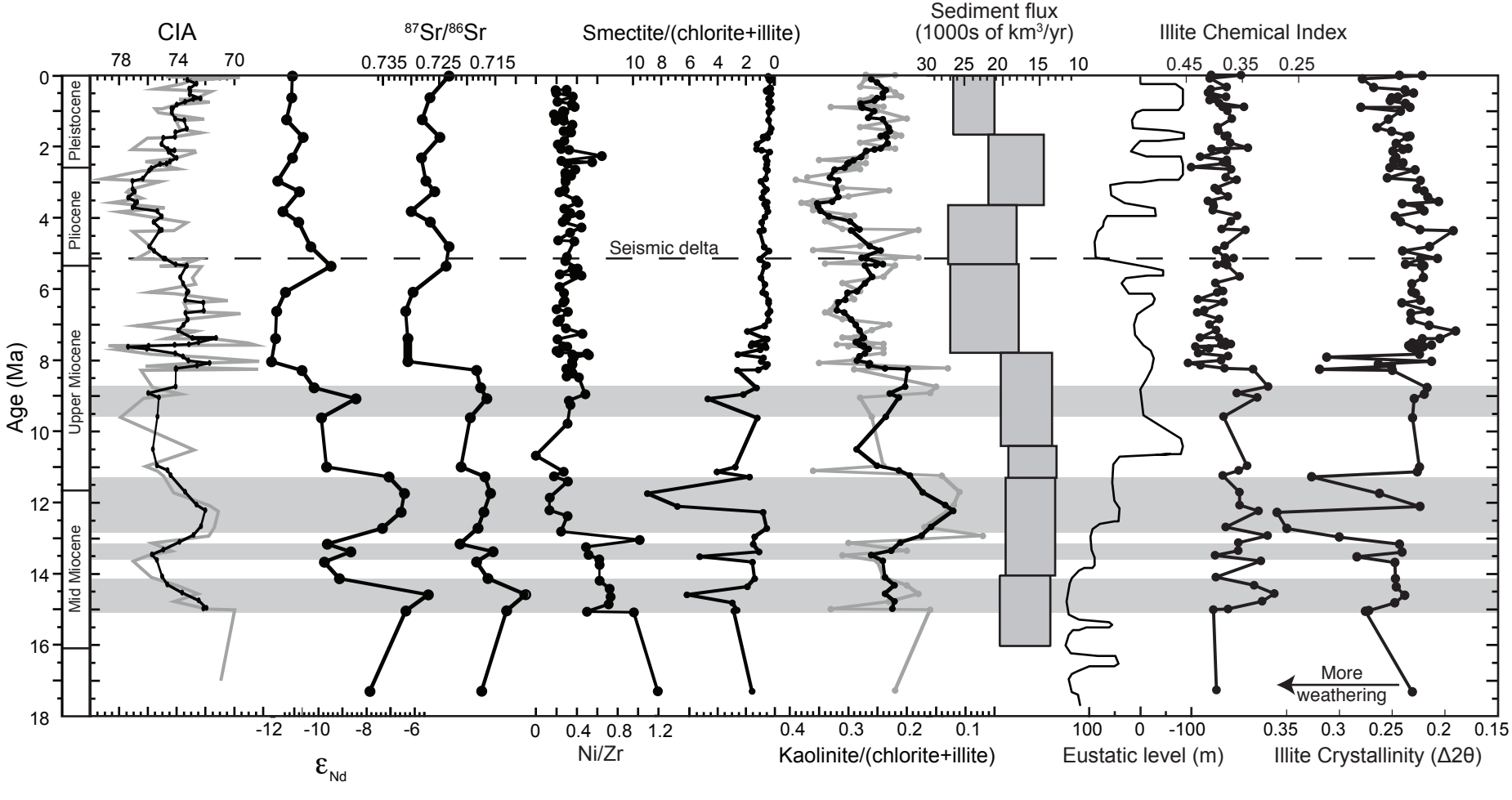

Figure 3
Liu et al.

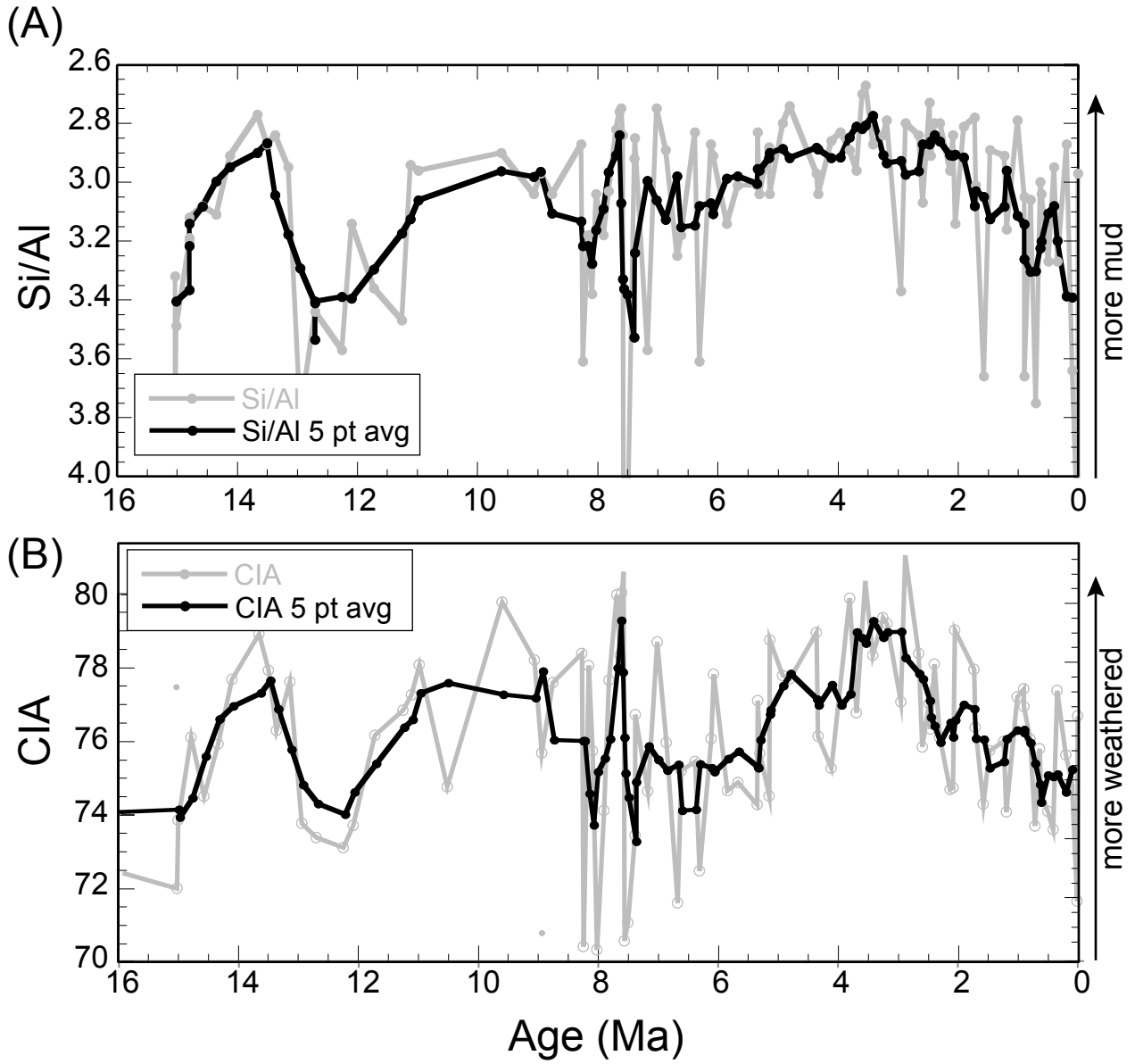

Figure 4
Liu et al.

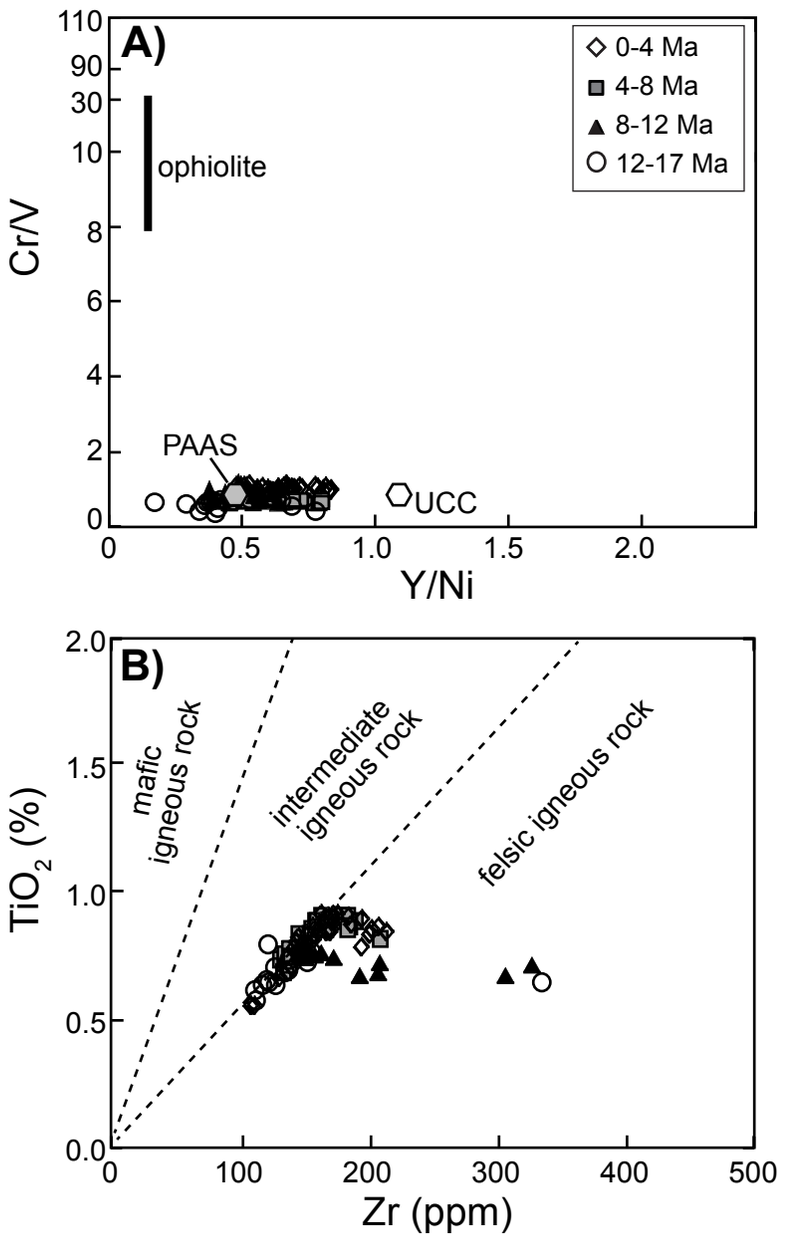

Liu et al.
Figure 5

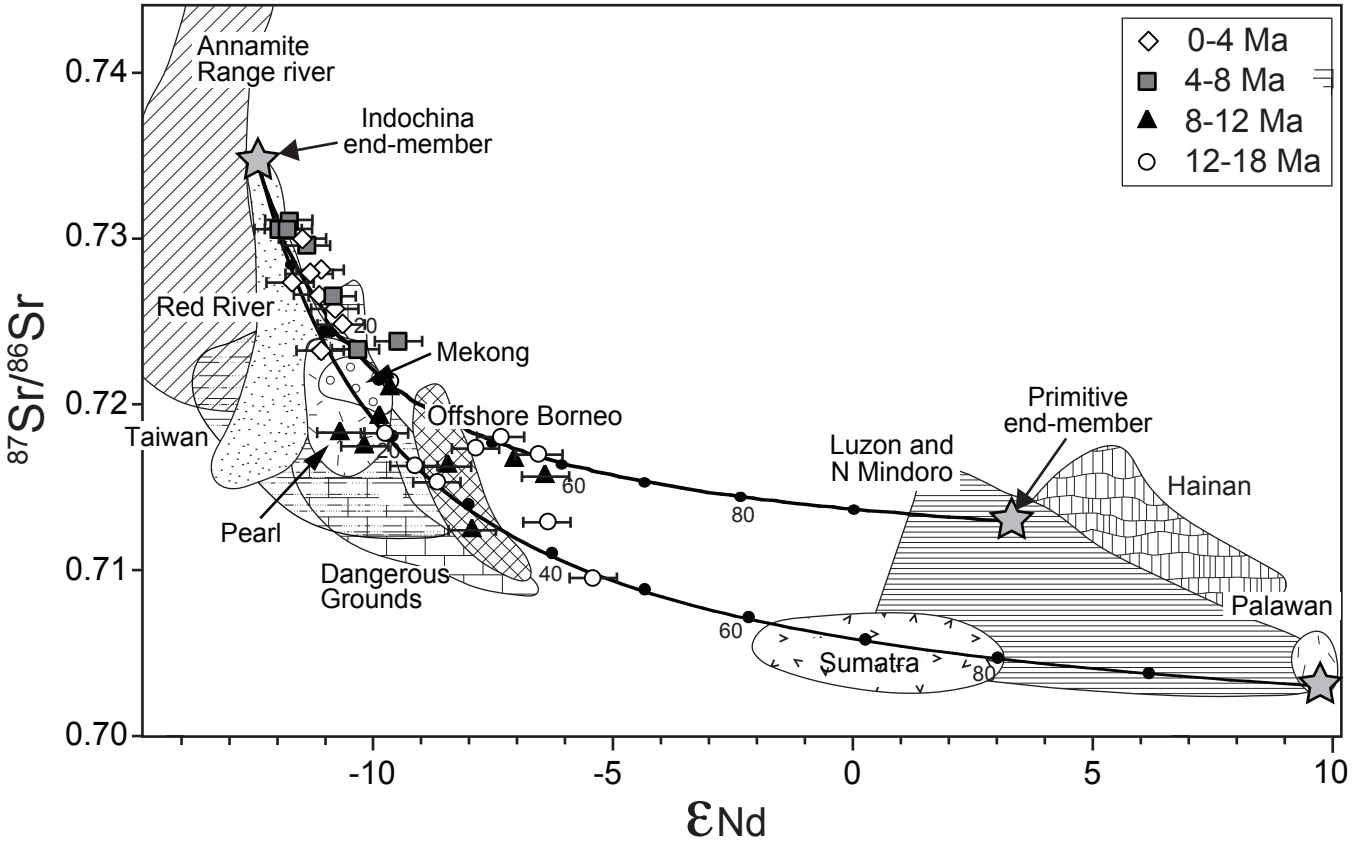

Figure 6
Liu et al.

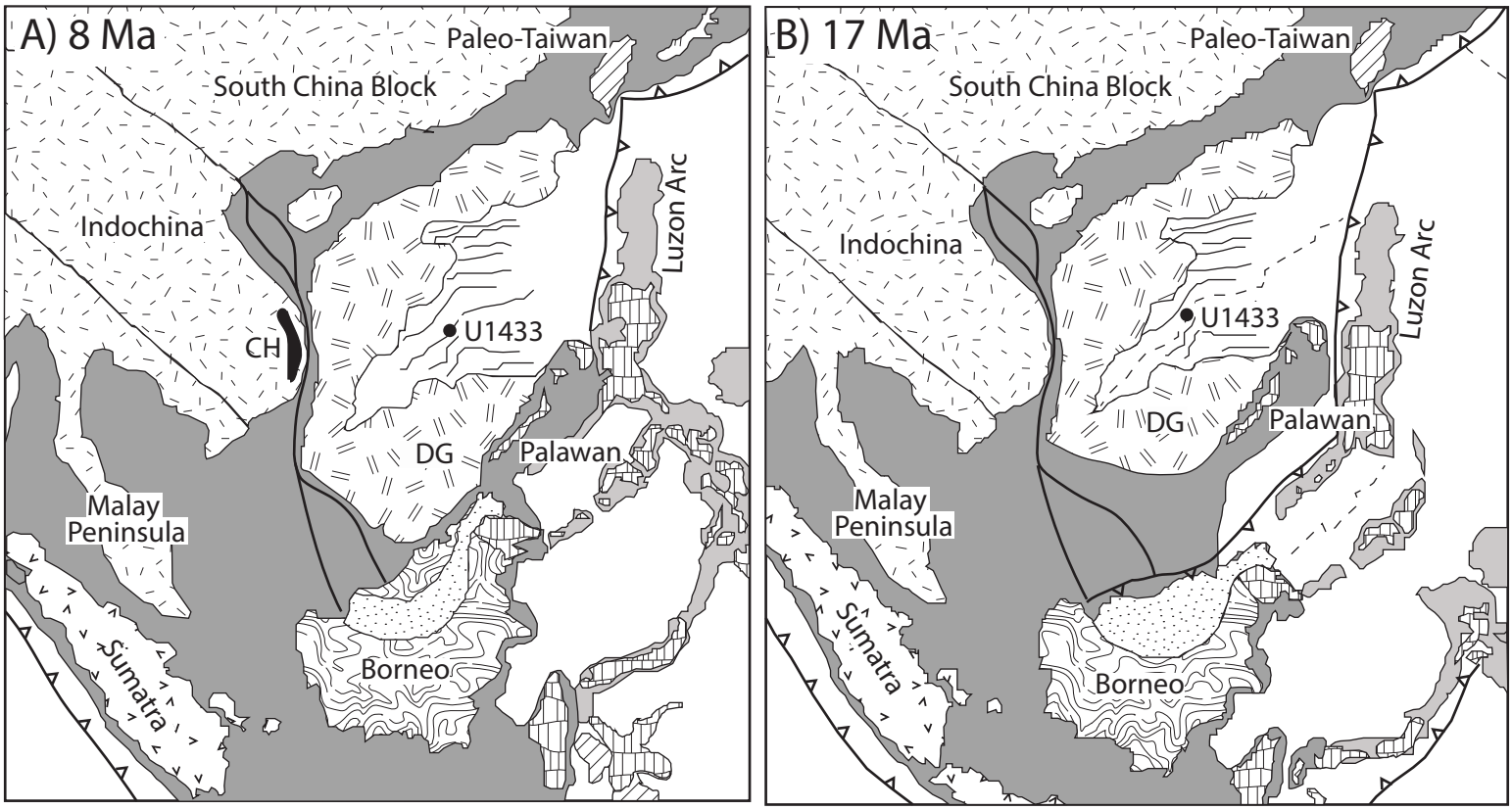

Figure 7
Liu et al.

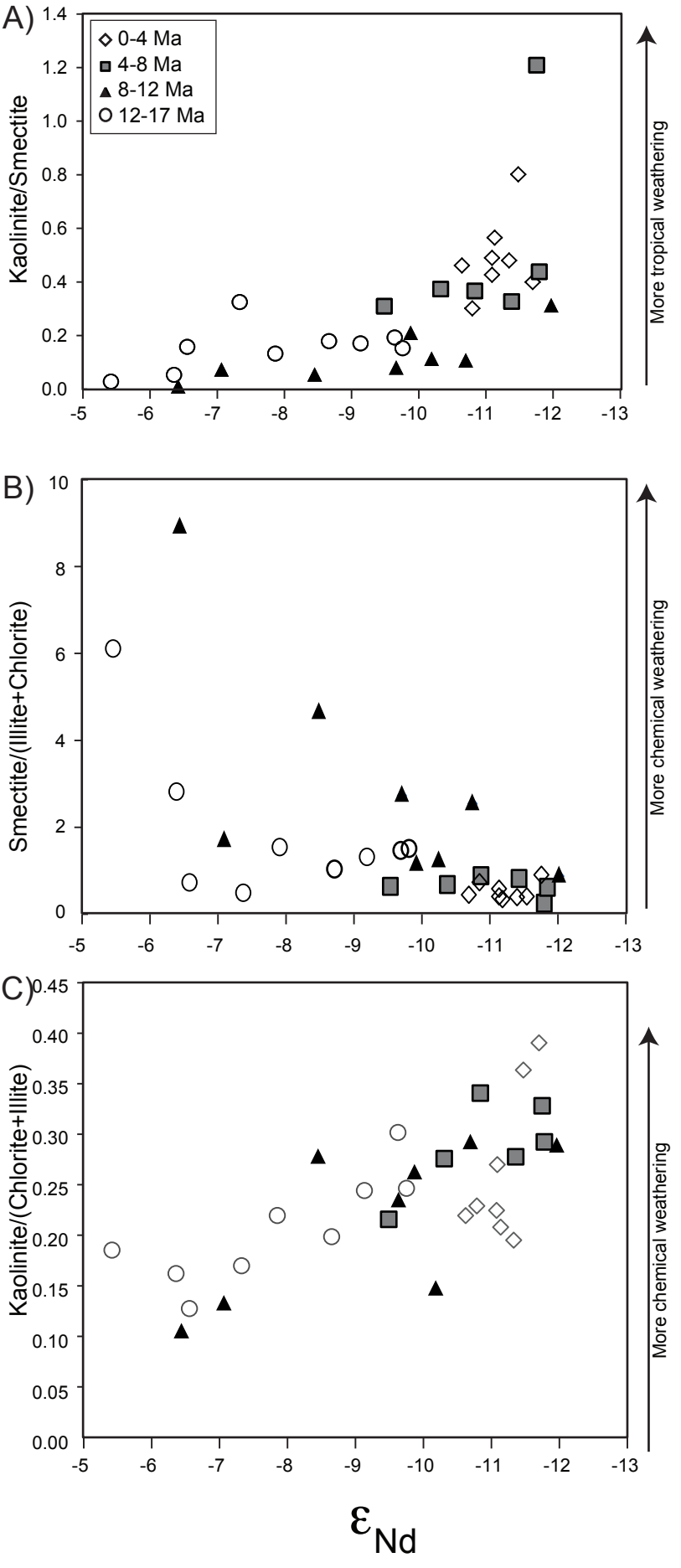

Figure 8
Liu et al.

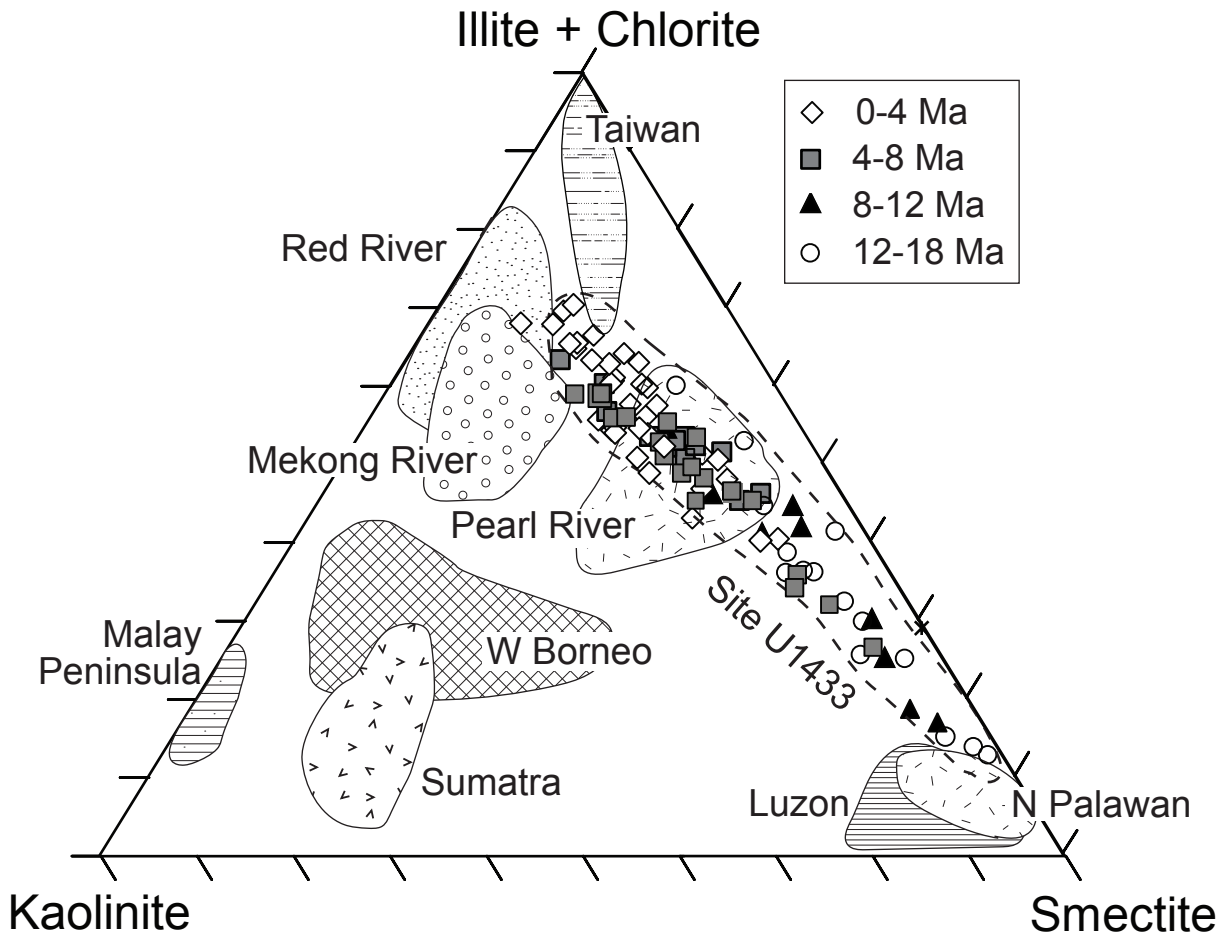

Figure 9
Liu et al.

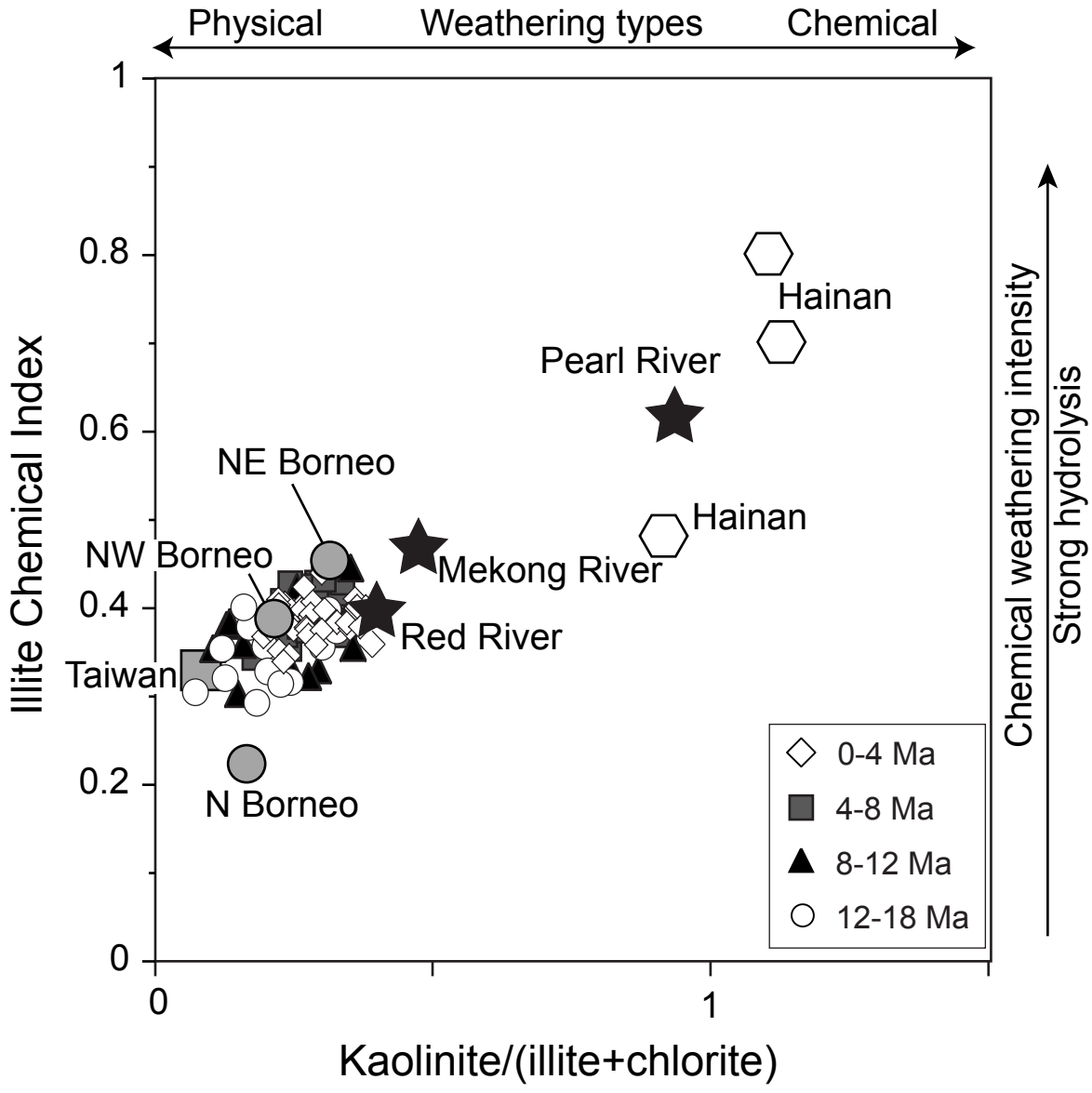

Figure 10
Liu et al.

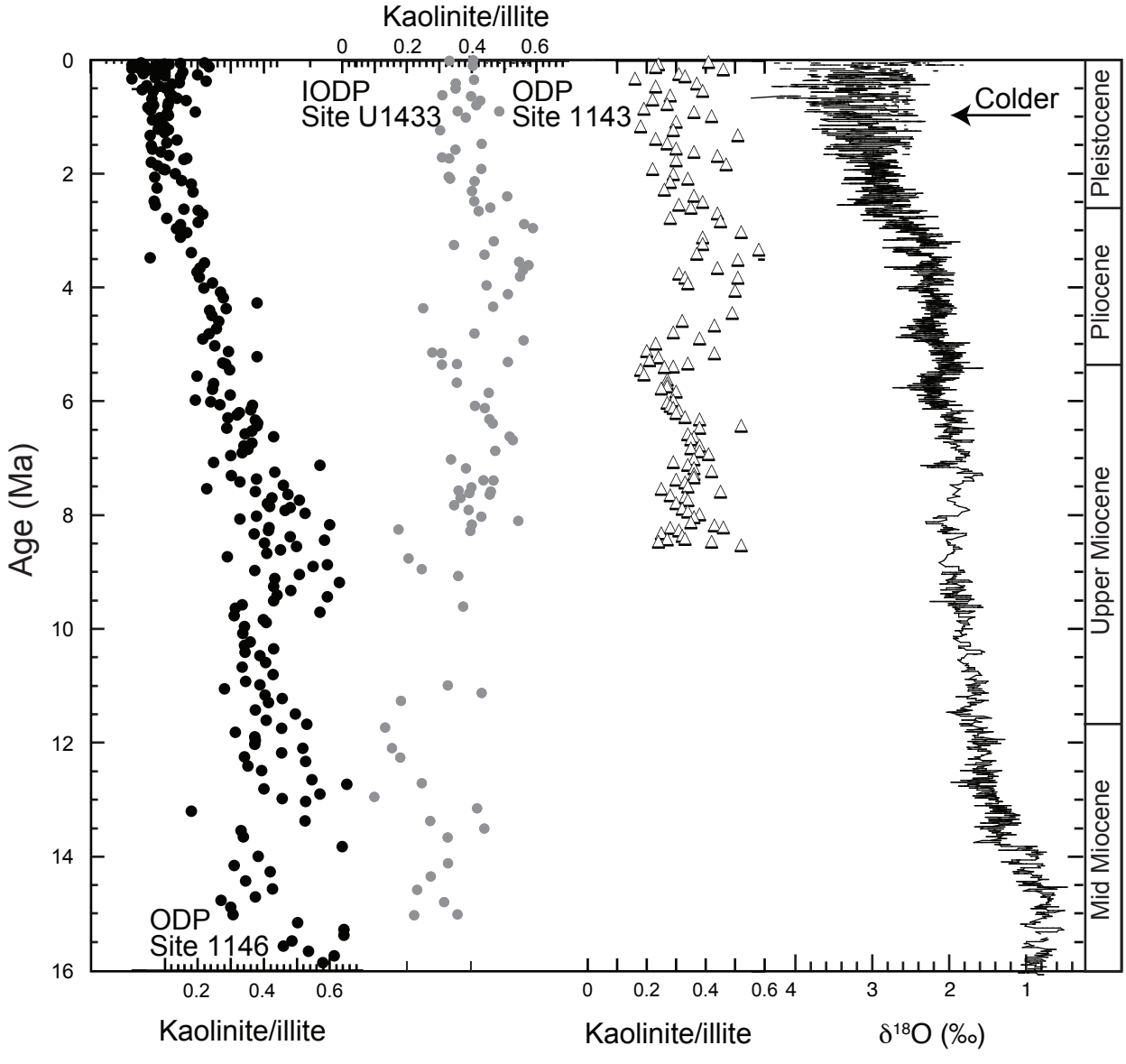

Figure 11
Liu et al.

Table 1

Sample	Age (Ma)	SiO_2	TiO_2	Al_2O_3	Fe_2O_3	MnO	MgO	CaO	Na_2O	K_2O	P_2O_5	Sr	Zr	Cu	Cr	V	Y	Ni	Sc	Ba
IODP U1433A																				
1H-1, 50-52 cm	0.00	55.97	0.85	18.82	6.99	0.06	2.36	0.58	0.68	3.28	0.13	99.8	162	40.3	98.3	139	29.8	48.8	17.5	639
1H-3, 50-52 cm	0.01	65.21	0.79	15.50	5.30	0.05	1.89	0.69	1.13	2.79	0.12	108.9	194	32.9	85.0	112	27.1	37.5	14.2	569
6H-5, 60-64 cm	0.10	62.79	0.86	17.25	6.13	0.05	1.97	0.56	0.90	3.04	0.12	103.3	203	34.5	88.2	125	34.0	40.4	16.2	473
8H-5, 48-52 cm	0.20	55.27	0.87	19.26	7.36	0.09	2.66	0.63	0.74	3.54	0.13	103.7	157	39.7	110.6	154	31.4	56.3	17.7	621
11H-1, 50-52 cm	0.34	59.94	0.88	18.33	5.55	0.04	1.91	0.43	0.71	3.15	0.12	95.8	186	31.4	96.5	125	30.5	39.1	16.8	481
13H-1, 50-54 cm	0.41	55.37	0.84	18.77	6.82	0.07	2.42	0.96	0.78	3.41	0.12	115.0	152	36.9	103.2	142	28.1	53.6	17.6	607
14H-5, 50-54 cm	0.50	57.14	0.85	17.46	8.48	0.06	2.24	0.73	0.82	3.17	0.13	105.5	167	35.9	102.2	133	30.3	63.2	16.1	572
16H-1, 50-54 cm	0.62	57.16	0.92	18.81	6.58	0.05	2.38	0.68	0.76	3.61	0.13	101.7	176	35.2	94.4	141	29.2	46.8	17.3	576
16H-3, 50-54 cm	0.63	57.88	0.85	19.28	6.76	0.06	2.34	0.67	0.76	3.41	0.13	105.7	170	39.7	100.7	146	30.6	47.4	17.1	545
17H-5, 50-54 cm	0.71	61.79	0.85	16.46	5.97	0.05	1.91	0.59	0.97	2.96	0.12	101.8	214	29.6	92.4	122	31.1	37.9	15.1	505
19H-1, 50-52 cm	0.79	57.34	0.86	18.74	6.65	0.06	2.23	0.51	0.74	3.46	0.11	94.8	170	34.5	109.0	143	30.0	45.4	17.6	545
IODP U1433B																				
2R-1, 34-36 cm	0.90	62.45	0.87	17.04	5.42	0.04	1.67	0.37	0.82	2.84	0.11	95.7	208	34.6	84.7	123	32.9	39.7	15.4	441
2R-1, 85-87 cm	0.90	60.79	0.91	19.92	7.01	0.06	2.22	0.48	0.75	3.43	0.12	102.0	184	38.7	91.4	138	34.2	49.7	18.2	521
4R-1, 24-28 cm	1.01	54.07	0.87	19.35	8.33	0.07	2.66	0.36	0.60	3.75	0.12	87.5	159	38.5	120.4	149	30.1	57.0	18.5	586
5R-3, 60-64 cm	1.19	59.33	0.91	18.77	7.16	0.06	2.57	0.74	0.90	3.46	0.14	107.3	173	32.5	119.0	148	31.6	46.9	17.9	604
5R-5, 60-64 cm	1.23	56.84	0.89	19.55	7.67	0.07	2.73	0.51	0.66	3.85	0.11	93.7	163	43.7	125.4	167	32.7	56.4	18.8	588
6R-2, 100-104 cm	1.47	56.06	0.90	19.41	7.05	0.06	2.40	0.60	0.72	3.64	0.12	101.3	165	31.8	110.5	149	31.3	45.7	17.8	613
6R-4, 30-34 cm	1.57	62.03	0.84	16.95	5.71	0.05	2.04	0.53	0.90	3.14	0.11	98.7	201	30.4	88.2	120	30.3	43.1	15.3	521
8R-2, 110-114 cm	1.71	56.81	0.82	18.90	7.32	0.04	2.54	0.56	0.60	3.55	0.09	100.8	157	31.8	96.3	144	26.8	38.7	17.6	561
8R-5, 50-54 cm	1.73	55.17	0.81	19.85	7.01	0.08	2.40	0.44	0.50	3.69	0.10	92.9	144	44.8	99.6	147	28.6	46.7	18.2	575
10R-3, 50-54 cm	1.91	41.93	0.56	14.92	5.90	0.21	2.43	13.08	0.50	2.38	0.56	722.7	111	111.0	97.2	126	36.4	71.5	16.1	588
12R-1, 36-38 cm	2.05	57.58	0.79	18.32	7.98	0.04	2.53	0.26	0.54	3.24	0.09	99.6	146	38.0	102.2	137	28.7	36.5	17.3	555
12R-4, 53-55 cm	2.08	52.70	0.71	18.55	7.36	0.05	2.57	1.21	0.47	3.03	0.45	175.5	140	105.3	99.5	156	42.5	77.3	19.3	539
13R-1, 78-82 cm	2.13	55.50	0.86	18.72	7.18	0.10	2.41	0.77	0.71	3.49	0.11	109.7	161	37.6	107.3	148	29.5	49.0	17.5	649
15R-3, 60-64 cm	2.30	54.44	0.77	19.43	7.23	0.07	2.47	0.98	0.46	3.28	0.21	141.6	147	66.4	84.1	143	32.4	56.4	18.1	571
16R-4, 110-114 cm	2.39	56.59	0.84	20.20	6.54	0.05	2.19	0.45	0.55	3.64	0.09	104.0	157	32.9	97.7	148	28.8	45.0	17.4	607
17R-3, 100-104 cm	2.46	56.14	0.91	19.29	6.83	0.06	2.30	0.61	0.59	3.60	0.09	110.7	171	37.4	107.3	145	31.7	49.6	18.0	648
17R-5, 114-118 cm	2.48	54.54	0.83	19.99	7.50	0.05	2.56	0.56	0.63	3.61	0.09	135.1	146	51.8	104.4	147	27.8	50.0	17.7	664
18R-2, 100-104 cm	2.59	58.91	0.91	19.17	6.82	0.05	2.36	0.63	0.69	3.54	0.11	110.6	168	35.9	97.3	146	29.9	49.0	17.5	662
18R-4, 50-54 cm	2.65	55.26	0.85	19.49	7.08	0.08	2.38	0.36	0.52	3.58	0.09	101.2	161	44.7	106.9	156	30.1	46.5	18.3	654

Table 1

Sample	Age (Ma)	SiO_2	TiO_2	Al_2O_3	Fe_2O_3	MnO	MgO	CaO	Na_2O	K_2O	P_2O_5	Sr	Zr	Cu	Cr	V	Y	Ni	Sc	Ba
IODP U1433B																				
19R 3, 71-75 cm	2.88	57.11	0.92	20.36	6.61	0.04	2.18	0.21	0.44	3.39	0.09	99.9	163	34.9	111.0	154	31.8	45.6	18.0	664
19R-5, 55-59 cm	2.95	60.26	0.90	17.87	6.07	0.04	2.04	0.61	0.52	3.09	0.08	108.0	195	26.5	90.8	125	32.7	44.7	16.3	588
20R-4, 90-94 cm	3.18	55.89	0.81	20.04	7.39	0.07	2.51	0.23	0.60	3.56	0.10	116.8	149	82.3	115.8	160	29.0	59.3	18.6	719
20R-6, 40-44 cm	3.25	55.46	0.77	19.55	7.22	0.06	2.58	0.27	0.54	3.43	0.09	126.9	143	65.9	89.2	149	28.3	59.2	17.7	661
21R-3, 141-143 cm	3.42	56.83	0.89	19.80	6.76	0.05	2.45	0.32	0.51	3.76	0.08	118.5	166	37.1	106.4	159	29.9	46.2	17.8	685
22R-1, 23-25 cm	3.54	53.76	0.79	20.10	8.15	0.10	2.58	0.31	0.44	3.35	0.09	104.5	143	67.1	90.8	145	29.7	47.7	18.3	671
23R-3, 145-149 cm	3.60	48.60	0.67	17.98	6.60	0.06	2.58	5.08	0.38	2.97	0.35	570.4	130	84.0	96.9	137	37.9	56.5	16.5	761
25R-5, 55-59 cm	3.69	56.39	0.89	19.08	6.72	0.05	2.09	0.58	0.55	3.52	0.09	122.3	165	28.5	88.7	142	30.1	48.8	17.3	662
26R-1, 50-54 cm	3.80	56.59	0.89	19.59	7.07	0.05	2.23	0.27	0.46	3.41	0.09	112.2	173	32.2	107.8	146	30.6	45.2	18.6	689
26R-3, 50-54 cm	3.96	42.27	0.56	14.96	6.60	0.66	2.33	10.65	0.35	2.71	0.70	677.3	108	154.7	90.4	129	38.8	48.1	14.4	523
26R-5, 50-54 cm	4.11	55.51	0.78	19.43	6.98	0.07	2.42	0.96	0.51	3.51	0.23	153.3	144	59.8	106.3	147	35.2	48.1	17.9	582
27R-1, 40-44 cm	4.33	58.06	0.89	19.10	6.34	0.04	2.19	0.56	0.57	3.72	0.09	140.3	172	28.7	93.6	142	30.1	37.6	17.5	693
27R-2, 15-19 cm	4.36	54.93	0.74	18.50	7.24	0.04	2.51	0.33	0.47	3.28	0.09	198.2	132	83.0	85.9	136	26.7	49.4	16.4	688
28R-1, 62-66 cm	4.80	55.38	0.79	20.19	6.99	0.04	2.35	0.57	0.48	3.67	0.10	146.9	148	71.7	96.5	149	29.7	45.1	17.7	668
28R-3, 48-52 cm	4.92	54.50	0.88	19.45	7.87	0.09	2.38	0.68	0.45	3.29	0.09	147.8	165	26.8	102.4	139	30.8	47.7	17.1	665
29R-1, 20-24 cm	5.14	55.74	0.79	18.32	7.42	0.04	2.57	0.31	0.49	3.31	0.09	197.1	147	55.1	97.5	154	27.1	60.1	17.1	636
29R-1, 71-75 cm	5.15	55.08	0.84	19.12	6.81	0.05	2.51	1.09	0.47	3.49	0.08	170.3	146	33.2	102.9	141	28.5	52.8	17.5	670
31R-1, 50-52 cm	5.30	57.15	0.90	18.82	7.07	0.07	2.36	0.71	0.58	3.52	0.10	149.0	170	30.2	107.6	146	31.9	39.7	17.8	658
33R-1, 101-103 cm	5.34	56.28	0.76	19.91	7.13	0.09	2.66	0.33	0.77	3.74	0.10	221.0	141	63.8	103.8	150	29.3	52.7	18.7	650
33R-5, 106-108 cm	5.35	55.20	0.69	18.34	6.59	0.04	2.60	1.01	0.48	3.45	0.25	124.6	134	87.4	104.3	144	34.8	59.6	17.8	398
34R-1, 26-28 cm	5.67	57.46	0.84	19.07	6.22	0.04	2.40	0.77	0.55	3.79	0.11	115.0	155	32.4	94.7	143	27.4	35.7	17.4	519
34R-3, 26-28 cm	5.85	57.45	0.87	18.29	6.81	0.09	2.35	0.84	0.61	3.40	0.09	136.8	168	32.1	111.1	139	29.7	45.9	16.6	552
35R-1, 39-41 cm	6.08	56.87	0.89	19.54	6.46	0.04	2.52	0.53	0.48	3.52	0.09	107.5	159	41.4	107.0	160	29.0	44.4	18.1	509
35R-3, 46-48 cm	6.12	55.60	0.86	19.35	6.75	0.05	2.49	0.69	0.53	3.65	0.12	121.8	167	38.1	111.8	147	29.6	44.9	17.7	556
36R-1, 40-44 cm	6.31	63.15	0.89	17.50	6.13	0.07	2.31	0.79	0.85	3.53	0.11	109.0	190	28.3	79.7	126	29.7	38.3	16.0	536
36R-3, 48-52 cm	6.38	54.18	0.84	19.15	7.66	0.08	2.42	0.88	0.51	3.50	0.10	144.6	155	36.3	114.7	143	30.5	48.4	17.8	552
37R-3, 78-82 cm	6.61	58.92	0.91	18.51	6.59	0.06	2.33	0.58	0.66	3.66	0.10	101.6	179	25.8	90.6	136	30.1	41.9	17.1	522
37R-5, 78-82 cm	6.68	58.44	0.91	17.98	6.75	0.07	2.38	1.09	0.74	3.63	0.10	154.4	184	27.2	83.5	133	30.6	38.7	16.1	554
38R-3, 94-98 cm	6.86	54.27	0.86	18.80	6.97	0.06	2.36	0.68	0.57	3.49	0.10	133.5	156	31.3	102.7	143	30.7	45.6	17.9	546
39R-1, 78-82 cm	7.02	55.82	0.78	20.30	7.76	0.05	2.57	0.29	0.48	3.86	0.10	337.2	140	41.2	90.5	143	28.9	63.8	18.1	565
39R-6, 66-69 cm	7.17	61.43	0.87	17.23	5.62	0.04	2.15	0.70	0.68	3.19	0.11	139.2	186	30.1	91.1	125	28.4	39.4	15.4	491
40R-5, 49-53 cm	7.38	56.07	0.91	19.67	6.61	0.05	2.45	0.49	0.54	3.86	0.10	109.6	164	33.0	98.5	151	28.3	43.7	18.2	510
40R-6, 5-9 cm	7.39	56.11	0.89	19.22	7.01	0.07	2.47	1.28	0.55	3.43	0.10	186.2	161	29.3	109.1	147	29.0	49.2	17.3	544

Table 1

Sample	Age (Ma)	SiO_2	TiO_2	Al_2O_3	Fe_2O_3	MnO	MgO	CaO	Na_2O	K_2O	P_2O_5	Sr	Zr	Cu	Cr	V	Y	Ni	Sc	Ba
IODP U1433B																				
43R-2, 119-122 cm	7.51	64.56	0.86	15.72	5.33	0.05	2.00	0.72	0.93	3.28	0.10	148.9	184	26.5	76.6	116	29.9	37.4	14.3	486
44R-3, 63-65 cm	7.56	64.12	0.82	15.29	5.07	0.05	1.85	0.97	0.86	2.95	0.12	155.4	209	35.5	82.5	115	33.0	47.7	13.2	503
44R-5, 48-50 cm	7.58	56.03	0.76	19.71	7.29	0.08	2.60	0.19	0.57	3.19	0.09	462.0	135	87.7	93.7	140	27.9	67.6	17.4	532
45R-1, 34-38 cm	7.61	55.62	0.77	20.20	7.31	0.11	2.52	0.22	0.46	3.59	0.10	254.3	142	87.9	121.5	159	30.1	50.6	18.8	617
45R-3, 89-93 cm	7.63	54.90	0.76	19.88	6.92	0.05	2.46	0.20	0.67	3.72	0.08	399.1	145	76.7	95.3	137	30.1	75.3	17.8	607
46R-2, 86-90 cm	7.69	56.67	0.78	20.08	7.02	0.05	2.60	0.21	0.52	3.51	0.09	428.1	139	126.4	104.3	141	28.5	51.2	17.9	617
48R-1, 103-107 cm	7.82	56.58	0.72	18.68	7.09	0.07	2.62	0.27	0.67	3.50	0.07	571.8	138	45.0	96.2	124	26.7	48.7	16.7	640
49R-3, 61-65 cm	7.91	56.93	0.75	17.89	6.10	0.04	2.10	1.00	0.46	3.40	0.08	185.2	140	58.0	100.5	149	25.5	49.8	16.3	527
51R-1, 35-38 cm	8.02	55.76	0.79	18.36	5.69	0.06	2.12	2.00	0.37	3.24	0.10	230.3	149	41.3	97.9	127	28.3	44.0	15.9	565
52R-1, 118-121 cm	8.10	59.73	0.76	17.66	6.18	0.05	1.98	0.59	0.66	3.22	0.09	213.1	159	64.5	108.0	128	27.2	55.0	16.0	529
53R-1, 40-42 cm	8.16	59.21	0.78	18.64	6.02	0.05	1.93	0.51	0.56	3.14	0.08	172.7	154	69.7	103.6	127	27.5	55.4	16.7	520
54R-2, 133-137 cm	8.25	60.84	0.75	16.87	5.07	0.03	1.96	1.33	0.78	3.12	0.06	326.2	151	48.4	79.9	123	25.9	45.3	15.3	435
54R-5, 85-89 cm	8.27	57.80	0.77	20.15	5.52	0.02	2.55	0.36	0.70	3.47	0.07	766.6	145	107.1	98.9	152	26.9	61.1	17.6	517
55R-3, 88-90 cm	8.76	57.60	0.75	18.96	6.96	0.04	2.49	0.33	0.69	3.46	0.06	876.7	151	124.4	71.4	127	28.0	72.6	16.9	522
55R-4, 98-100 cm	8.94	57.39	0.69	19.35	6.19	0.03	2.37	0.34	1.14	3.45	0.08	922.6	208	103.6	77.9	129	31.6	66.9	16.0	500
55R-5, 60-62 cm	9.07	56.86	0.68	18.73	5.85	0.04	2.46	0.38	0.88	2.85	0.06	1032.0	194	59.9	73.5	103	24.7	65.2	15.0	730
56R-1, 80-84 cm	9.60	56.33	0.75	19.42	6.06	0.03	2.23	0.28	0.53	3.28	0.06	832.1	173	64.0	91.6	131	33.1	53.6	16.8	533
57R-2, 67-70 cm	10.52	52.99	0.64	17.41	5.45	0.03	2.38	0.71	0.69	3.19		832.8		93.0		114	27.9		15.2	492
57R-6, 85-89 cm	10.99	59.11	0.73	20.00	6.73	0.07	2.53	0.40	0.62	3.57	0.06	898.6	209	73.2	77.6	142	32.7	56.5	17.9	558
58R-1, 37-41 cm	11.12	56.42	0.72	19.18	5.96	0.05	2.51	0.42	0.82	3.27	0.08	905.2	328	90.6	72.7	144	36.8	57.5	16.8	985
58R-2, 73-77 cm	11.26	60.37	0.77	17.39	5.08	0.02	1.97	0.20	0.76	3.34	0.07	507.5	164	60.5	87.6	132	28.4	51.2	16.2	502
58R-6, 91-95 cm	11.73	59.17	0.68	17.61	4.83	0.02	2.60	0.75	0.60	2.92	0.06	495.7	307	71.8	88.9	111	21.5	41.6	13.9	454
59R-3, 59-61 cm	12.09	57.98	0.65	18.47	5.81	0.02	2.88	0.50	1.37	3.16	0.09	798.1	335	83.5	43.5	111	34.1	43.7	14.3	538
59R-4, 130-133 cm	12.26	60.70	0.77	16.98	5.73	0.04	1.97	0.67	0.84	3.36	0.07	194.2	156	50.2	91.1	128	25.7	48.4	15.9	408
60R-2, 45-47 cm	12.71	59.20	0.76	17.21	5.82	0.06	2.03	0.63	0.78	3.52	0.07	139.6	150	46.2	63.8	121	25.5	36.8	16.0	377
60R-4, 74-76 cm	12.95	59.65	0.70	15.76	7.53	0.07	2.29	0.20	0.93	3.43	0.07	317.5	138	71.1	71.7	113	24.3	140.2	14.8	537
60R-6, 37-39 cm	13.15	57.12	0.74	19.34	7.36	0.08	2.45	0.24	0.82	3.50	0.09	358.1	138	47.5	85.9	129	31.8	68.0	18.7	1188
61R-1, 102-104 cm	13.37	54.88	0.73	19.33	7.44	0.16	2.28	0.28	0.91	3.70	0.09	317.1	152	79.7	83.2	122	30.8	78.4	17.2	1031
61R-2, 131-135 cm	13.50	56.02	0.69	19.53	7.28	0.26	2.32	0.31	0.86	3.27	0.10	312.8	135	56.8	81.1	125	31.7	83.8	17.7	825
61R-4, 39-43 cm	13.66	54.75	0.71	19.76	7.48	0.13	2.25	0.27	0.66	3.42	0.06	273.4	127	85.1	83.5	133	29.8	79.6	17.7	835
62R-1, 112-116 cm	14.12	54.95	0.66	18.90	7.29	0.43	2.10	0.42	0.69	3.27	0.10	230.2	121	202.9	80.5	115	31.8	75.5	17.3	773
62R-3, 113-117 cm	14.35	56.02	0.64	18.03	7.26	0.08	2.28	0.41	0.84	3.32	0.07	227.7	118	109.6	76.1	138	30.1	84.8	16.9	946
62R-5, 119-123 cm	14.58	57.37	0.80	18.65	4.92	0.05	2.56	1.08	1.12	2.38	0.07	300.7	122	6077.8	67.3	174	30.3	89.1	22.0	767

Table 1

Sample	Age (Ma)	SiO_2	TiO_2	Al_2O_3	Fe_2O_3	MnO	MgO	CaO	Na_2O	K_2O	P_2O_5	Sr	Zr	Cu	Cr	V	Y	Ni	Sc	Ba
IODP U1433B																				
63R-1, 39-43 cm	14.80	55.86	0.65	17.92	8.00	0.09	2.35	0.48	0.83	3.13	0.09	206.7	123	62.7	76.9	163	35.6	87.3	16.9	999
63R-4, 112-116 cm	15.01	57.84	0.64	16.58	8.57	0.17	2.39	0.52	0.92	3.15	0.08	182.3	128	82.7	77.5	113	41.5	63.8	16.2	1096
64R-1, 50-54 cm	15.03	55.99	0.58	14.61	9.49	0.35	2.90	0.71	0.81	2.83	0.09	189.5	113	97.3	67.0	201	43.8	108.4	15.5	2229
65R-1, 57-61 cm	17.29	51.93	0.62	15.62	10.60	1.63	3.15	0.69	0.48	3.36	0.08	198.0	112	311.0	73.7	126	38.6	133.3	15.9	717

Table 2

Sample	Age (Ma)	Smectite (%)	Chlorite (%)	Illite (%)	Kaolinite (%)	Illite Crystallinity	Illite Chemistry Index
IODP U1433A							
1H-1, 50-52 cm	0.00	23.2	20.8	39.6	16.3	0.243	0.406
1H-3, 50-52 cm	0.01	26.2	20.1	40.2	13.5	0.222	0.353
6H-5, 60-64 cm	0.10	17.1	22.3	43.0	17.6	0.278	0.408
11H-1, 50-52 cm	0.34	17.1	21.5	43.4	18.0	0.268	0.378
13H-1, 50-54 cm	0.41	29.3	19.6	37.7	13.4	0.238	0.406
14H-5, 50-54 cm	0.50	14.2	26.1	44.0	15.6	0.230	0.411
16H-1, 50-54 cm	0.62	22.4	21.6	42.6	13.4	0.245	0.379
16H-3, 50-54 cm	0.63	23.1	21.1	39.7	16.1	0.251	0.400
17H-5, 50-54 cm	0.71	16.4	22.5	42.6	18.5	0.252	0.408
19H-1, 50-52 cm	0.79	23.2	20.4	39.7	16.7	0.238	0.391
IODP U1433B							
2R-1, 34-36 cm	0.90	13.4	23.1	46.6	16.9	0.233	0.347
2R-1, 85-87 cm	0.90	10.0	22.9	44.9	22.2	0.280	0.385
4R-1, 24-28 cm	1.01	21.7	22.2	40.4	15.7	0.242	0.377
5R-5, 60-64 cm	1.23	24.5	22.7	40.5	12.4	0.254	0.369
6R-2, 100-104 cm	1.47	13.3	24.4	43.3	19.0	0.265	0.394
6R-4, 30-34 cm	1.57	18.0	23.5	43.2	15.3	0.251	0.393
8R-2, 110-114 cm	1.71	39.1	16.6	33.8	10.5	0.233	0.377
8R-5, 50-54 cm	1.73	27.0	20.7	39.2	13.1	0.236	0.381
10R-3, 50-54 cm	1.91	48.7	14.4	25.7	11.3	0.246	0.372
12R-1, 36-38 cm	2.05	50.3	12.2	28.1	9.4	0.235	0.340
12R-4, 53-55 cm	2.08	41.2	16.3	31.8	10.8	0.240	0.405
13R-1, 78-82 cm	2.13	19.7	21.8	41.3	17.2	0.249	0.379
15R-3, 60-64 cm	2.30	32.0	18.3	35.3	14.4	0.247	0.425
16R-4, 110-114 cm	2.39	26.4	17.7	36.7	19.1	0.249	0.378
17R-3, 100-104 cm	2.46	26.0	19.1	35.9	19.0	0.240	0.384
17R-5, 114-118 cm	2.48	28.8	19.1	36.8	15.3	0.241	0.377
18R-2, 100-104 cm	2.59	30.1	19.0	34.7	16.2	0.252	0.441
18R-4, 50-54 cm	2.65	26.3	20.5	37.2	16.0	0.228	0.370
19R 3, 71-75 cm	2.88	30.6	18.0	32.6	18.7	0.255	0.380
19R-5, 55-59 cm	2.95	40.0	15.2	28.0	16.9	0.223	0.360
20R-4, 90-94 cm	3.18	28.9	19.6	34.8	16.6	0.227	0.399
20R-6, 40-44 cm	3.25	36.9	17.8	33.5	11.7	0.220	0.393
21R-3, 141-143 cm	3.42	39.2	15.4	31.4	14.0	0.216	0.376
22R-1, 23-25 cm	3.54	26.0	19.3	35.1	19.6	0.206	0.411
23R-3, 145-149 cm	3.60	32.8	17.3	31.4	18.5	0.241	0.402
25R-5, 55-59 cm	3.69	26.7	19.7	34.1	19.5	0.224	0.401
26R-1, 50-54 cm	3.80	24.0	19.6	36.1	20.3	0.220	0.403
26R-3, 50-54 cm	3.96	32.7	18.8	33.3	15.2	0.247	0.359
26R-5, 50-54 cm	4.11	39.7	15.6	29.3	15.3	0.242	0.371

Table 2

Sample	Age (Ma)	Smectite (%)	Chlorite (%)	Illite (%)	Kaolinite (%)	Illite Crystallinity	Illite Chemistry Index
IODP U1433B							
27R-1, 40-44 cm	4.33	36.0	16.4	32.2	15.3	0.224	0.387
27R-2, 15-19 cm	4.36	45.5	13.1	33.0	8.3	0.192	0.345
28R-1, 62-66 cm	4.80	35.4	17.1	33.5	14.0	0.215	0.382
28R-3, 48-52 cm	4.92	19.9	21.6	37.2	21.3	0.240	0.396
29R-1, 20-24 cm	5.14	45.6	16.5	29.6	8.3	0.207	0.380
29R-1, 71-75 cm	5.15	45.0	13.9	31.3	9.7	0.223	0.366
31R-1, 50-52 cm	5.30	25.3	19.5	36.3	19.0	0.238	0.383
33R-1, 101-103 cm	5.34	31.3	17.7	37.5	13.5	0.220	0.395
33R-5, 106-108 cm	5.35	35.2	16.4	36.9	11.5	0.222	0.377
34R-1, 26-28 cm	5.67	42.3	15.1	31.3	11.3	0.221	0.355
34R-3, 26-28 cm	5.85	33.1	16.2	34.7	16.0	0.232	0.398
35R-1, 39-41 cm	6.08	38.6	16.2	31.9	13.3	0.231	0.384
35R-3, 46-48 cm	6.12	31.7	17.9	34.8	15.6	0.228	0.395
36R-1, 40-44 cm	6.31	22.3	22.2	37.9	17.6	0.223	0.429
36R-3, 48-52 cm	6.38	22.6	19.6	39.2	18.6	0.241	0.384
37R-3, 78-82 cm	6.61	16.2	24.2	39.0	20.6	0.215	0.418
37R-5, 78-82 cm	6.68	24.3	21.1	35.5	19.1	0.233	0.430
38R-3, 94-98 cm	6.86	23.1	20.9	37.8	18.2	0.233	0.391
39R-1, 78-82 cm	7.02	35.7	16.8	35.4	12.1	0.215	0.409
39R-6, 66-69 cm	7.17	60.2	10.6	21.0	8.2	0.190	0.397
40R-5, 49-53 cm	7.38	32.8	17.9	34.1	15.2	0.205	0.426
40R-6, 5-9 cm	7.39	27.1	19.6	36.1	17.2	0.222	0.392
43R-2, 119-122 cm	7.51	54.9	11.9	23.6	9.6	0.231	0.380
44R-3, 63-65 cm	7.56	34.0	18.9	34.5	12.6	0.213	0.371
44R-5, 48-50 cm	7.58	55.4	10.9	23.0	10.7	0.235	0.387
45R-1, 34-38 cm	7.61	33.3	18.3	34.6	13.8	0.221	0.380
45R-3, 89-93 cm	7.63	30.3	18.4	35.0	16.3	0.233	0.434
46R-2, 86-90 cm	7.69	43.8	15.5	29.7	11.0	0.228	0.409
48R-1, 103-107 cm	7.82	67.4	8.0	18.3	6.4	0.224	0.429
49R-3, 61-65 cm	7.91	37.1	15.0	34.2	13.6	0.312	0.376
51R-1, 35-38 cm	8.02	40.7	15.3	30.6	13.4	0.213	0.388
52R-1, 118-121 cm	8.10	24.9	20.3	35.2	19.6	0.263	0.447
53R-1, 40-42 cm	8.16	31.7	20.1	34.2	13.9	0.251	0.425
54R-2, 133-137 cm	8.25	49.8	11.2	33.3	5.8	0.319	0.382
54R-5, 85-89 cm	8.27	66.5	6.9	18.9	7.6	0.250	0.331
55R-3, 88-90 cm	8.76	52.0	11.2	30.5	6.3	0.217	0.304
55R-4, 98-100 cm	8.94	65.2	10.6	19.4	4.8	0.220	0.360
55R-5, 60-62 cm	9.07	78.7	4.0	12.7	4.6	0.229	0.324
56R-1, 80-84 cm	9.60	48.3	12.7	28.3	10.7	0.231	0.384
57R-6, 85-89 cm	10.99	69.1	7.0	18.0	5.9	0.224	0.342
58R-1, 37-41 cm	11.12	75.0	3.5	15.0	6.6	0.226	0.357

Table 2

Sample	Age (Ma)	Smectite (%)	Chlorite (%)	Illite (%)	Kaolinite (%)	Illite Crystallinity	Illite Chemistry Index
IODP U1433B							
58R-2, 73-77 cm	11.26	60.4	8.7	26.2	4.7	0.327	0.385
58R-6, 91-95 cm	11.73	89.1	1.9	8.0	1.0	0.262	0.355
59R-3, 59-61 cm	12.09	86.0	2.5	10.1	1.5	0.224	0.355
59R-4, 130-133 cm	12.26	40.5	15.0	37.7	6.7	0.359	0.321
60R-2, 45-47 cm	12.71	29.9	18.4	41.4	10.3	0.350	0.380
60R-4, 74-76 cm	12.95	55.8	9.2	32.0	3.1	0.300	0.305
60R-6, 37-39 cm	13.15	53.3	10.4	25.5	10.8	0.243	0.357
61R-1, 102-104 cm	13.37	46.8	12.3	32.2	8.8	0.241	0.357
61R-2, 131-135 cm	13.50	80.1	4.6	10.6	4.7	0.284	0.399
61R-4, 39-43 cm	13.66	55.0	9.3	26.8	8.9	0.248	0.317
62R-1, 112-116 cm	14.12	52.2	10.1	28.4	9.4	0.247	0.397
62R-3, 113-117 cm	14.35	61.3	8.4	23.8	6.6	0.246	0.329
62R-5, 119-123 cm	14.58	84.0	2.8	10.7	2.5	0.238	0.293
63R-1, 39-43 cm	14.80	70.7	6.9	17.0	5.4	0.248	0.315
63R-4, 112-116 cm	15.01	66.3	2.4	23.0	8.3	0.272	0.376
64R-1, 50-54 cm	15.03	71.2	6.9	17.9	4.0	0.276	0.402
65R-1, 57-61 cm	17.29	56.2	12.4	23.6	7.9	0.231	0.396

Table 3

Sample	Age (Ma)	$^{87}Sr/^{86}Sr$	$^{143}Nd/^{144}Nd$	Epsilon Nd
IODP U1433A				
1H-3, 50-52 cm	0.01	0.723270	0.512070	-11.1
16H-1, 50-54 cm	0.62	0.726637	0.512068	-11.1
IODP U1433B				
5R-5, 60-64 cm	1.23	0.728032	0.512057	-11.3
8R-5, 50-54 cm	1.73	0.724873	0.512093	-10.6
15R-3, 60-64 cm	2.30	0.728157	0.512070	-11.1
19R-5, 55-59 cm	2.95	0.727383	0.512039	-11.7
20R-6, 40-44 cm	3.25	0.725789	0.512085	-10.8
26R-1, 50-54 cm	3.80	0.729998	0.512050	-11.5
26R-5, 50-54 cm	4.11	0.726594	0.512083	-10.8
28R-1, 62-66 cm	4.80	0.723252	0.512109	-10.3
33R-5, 106-108 cm	5.35	0.723778	0.512152	-9.5
35R-1, 39-41 cm	6.08	0.729627	0.512055	-11.4
37R-3, 78-82 cm	6.61	0.730936	0.512036	-11.7
40R-5, 49-53 cm	7.38	0.730567	0.512034	-11.8
40R-5, 49-53 cm	7.38	0.730525	0.512023	-12.0
40R-5, 49-53 cm	7.38		0.512036	-11.7
51R-1, 35-38 cm	8.02	0.730567	0.512025	-12.0
54R-5, 85-89 cm	8.27	0.718308	0.512090	-10.7
55R-3, 88-90 cm	8.76	0.717633	0.512116	-10.2
55R-5, 60-62 cm	9.07	0.716482	0.512205	-8.4
56R-1, 80-84 cm	9.60	0.719418	0.512132	-9.9
57R-2, 67-70 cm	10.52	0.712584	0.512231	-7.9
57R-6, 85-89 cm	10.99	0.721065	0.512143	-9.7
58R-2, 73-77 cm	11.26	0.716830	0.512276	-7.1
58R-6, 91-95 cm	11.73	0.715851	0.512309	-6.4
59R-4, 130-133 cm	12.26	0.717045	0.512302	-6.6
60R-2, 45-47 cm	12.71	0.718080	0.512262	-7.3
60R-6, 37-39 cm	13.15	0.721289	0.512144	-9.6
61R-1, 102-104 cm	13.37	0.715412	0.512194	-8.7
61R-4, 39-43 cm	13.66	0.718294	0.512138	-9.8
61R-4, 39-43 cm	14.66	0.718332	0.512147	-9.6
61R-4, 39-43 cm	15.66		0.512139	-9.7
62R-1, 112-116 cm	14.12	0.716304	0.512170	-9.1
62R-5, 119-123 cm	14.58	0.709552	0.512360	-5.4
64R-1, 50-54 cm	15.03	0.712963	0.512312	-6.4
65R-1, 57-61 cm	17.29	0.717409	0.512235	-7.9

Table S1

Sample	SiO_2	TiO_2	Al_2O_3	Fe_2O_3	MnO	MgO	CaO	Na_2O	K_2O	P_2O_5	Sr	Zr	Cu	Cr	V	Y	Ni	Sc	Ba
Replicas																			
60R 2W 1	59.20	0.76	17.21	5.82	0.06	2.03	0.63	0.78	3.52	0.07	139.6	150.2	46.2	63.8	121.1	25.5	36.8	16.0	377
60R 2W 2	60.02	0.77	17.42	5.89	0.06	2.05	0.64	0.79	3.46	0.07	141.6	150.7	43.9	71.2	127.2	25.0	39.0	15.9	385
60R 2W 3	60.78	0.78	17.65	5.96	0.06	2.09	0.64	0.80	3.58	0.08	144.4	153.6	52.8	83.3	132.5	26.5	45.2	16.1	376
63R 1W 1	55.86	0.65	17.92	8.00	0.09	2.35	0.48	0.83	3.13	0.09	206.7	122.8	62.7	76.9	163.2	35.6	87.3	16.9	999
63R 1W 2	57.32	0.65	17.96	8.04	0.09	2.37	0.48	0.85	3.27	0.09	207.3	120.4	53.1	83.4	162.7	35.2	88.9	16.7	1004
63R 1W 3	57.56	0.66	17.96	8.11	0.09	2.38	0.48	0.85	3.33	0.10	207.8	125.0	56.4	87.4	163.8	35.4	89.5	16.9	1003
M1	55.97	0.79	18.51	7.01	0.11	2.52	1.27	0.71	3.52	0.11	232.5	150.0	131.1	91.1	137.9	29.7	58.3	17.3	608
M2	56.09	0.79	18.55	6.97	0.11	2.54	1.23	0.71	3.64	0.11	232.1	149.1	131.5	107.7	142.9	29.2	56.5	17.0	613
M3	57.09	0.80	18.78	7.03	0.11	2.55	1.23	0.71	3.44	0.12	233.6	150.8	127.7	100.4	142.4	30.9	54.2	17.3	606
60R 2W Replicates																			
Average	60.00	0.77	17.43	5.89	0.06	2.06	0.64	0.79	3.52	0.07	141.9	151.5	47.6	72.8	126.9	25.7	40.3	16.0	380
Standard deviation	0.79	0.01	0.22	0.07	0.00	0.03	0.01	0.01	0.06	0.01	2.4	1.9	4.6	9.8	5.7	0.7	4.4	0.1	5.0
% relative standard deviation	1.31	1.32	1.24	1.17	1.40	1.42	0.97	1.25	1.67	6.97	1.7	1.2	9.6	13.5	4.5	2.9	10.8	0.7	1.3
63R 1W Replicates																			
average	56.91	0.66	17.95	8.05	0.09	2.37	0.48	0.84	3.24	0.09	207.3	122.8	57.4	82.6	163.2	35.4	88.6	16.8	1002
stdev	0.92	0.00	0.02	0.06	0.00	0.02	0.00	0.01	0.11	0.01	0.5	2.3	4.9	5.3	0.5	0.2	1.1	0.1	2.5
%rsd	1.61	0.13	0.12	0.70	0.31	0.68	0.40	1.08	3.26	6.15	0.3	1.9	8.5	6.4	0.3	0.5	1.3	0.6	0.3
M Replicates																			
Average	56.38	0.79	18.61	7.00	0.11	2.53	1.24	0.71	3.53	0.11	232.7	150.0	130.1	99.7	141.1	29.9	56.3	17.2	609
Standard deviation	0.62	0.01	0.14	0.03	0.00	0.02	0.02	0.00	0.10	0.00	0.7	0.8	2.1	8.3	2.7	0.9	2.1	0.2	3.6
% relative standard deviation	1.09	0.89	0.77	0.41	1.36	0.60	1.72	0.34	2.82	0.82	0.3	0.6	1.6	8.3	1.9	2.8	3.7	1.0	0.6
Standard																			
BHVO-2-1	49.62	2.70	13.53	12.19	0.17	7.16	11.15	2.20	0.51	0.28	395.3	169.7	134.9	320.4	317.7	26.8	116.0	31.1	144
BHVO-2-2	49.12	2.71	13.76	12.18	0.16	7.17	11.21	2.23	0.52	0.28	398.0	169.0	124.6	302.2	321.1	28.1	113.5	31.2	131
BHVO-2-3	49.80	2.73	13.78	12.08	0.17	7.26	11.34	2.24	0.51	0.27	398.1	172.2	132.4	309.5	320.2	27.4	112.9	32.2	133
BHVO-2-4	49.82	2.75	13.78	12.08	0.17	7.23	11.25	2.16	0.48	0.29	398.1	167.0	132.4	289.8	312.3	25.7	106.1	30.8	128
BHVO-2-5	51.12	2.78	13.99	12.41	0.17	7.31	11.41	2.27	0.53	0.27	403.5	177.8	139.5	295.7	320.2	27.8	113.0	31.9	135
BHVO-2-6	50.54	2.77	13.87	12.16	0.17	7.29	11.37	2.30	0.51	0.28	400.0	168.8	138.6	297.3	318.6	28.5	103.8	31.5	134
Standard																			
Average	50.00	2.74	13.78	12.18	0.17	7.24	11.29	2.23	0.51	0.28	398.8	170.8	133.8	302.5	318.4	27.4	110.9	31.5	134
Standard deviation	0.71	0.03	0.15	0.12	0.00	0.06	0.10	0.05	0.02	0.01	2.7	3.8	5.4	11.0	3.2	1.0	4.8	0.5	5.4
% relative standard deviation	1.43	1.15	1.10	0.98	0.76	0.84	0.92	2.11	3.13	3.43	0.7	2.2	4.0	3.6	1.0	3.6	4.3	1.7	4.0

Background dataset for online publication only

Click here to download Background dataset for online publication only: Table_S1_U1433_Geochemical Data_suplimental materi